Analysis of a Tunable CMOS-compatible Multilayer Waveguide Structure for Dual Polarizer-modulator Operation

Renan Silva Santos (renan.santos@aluno.cefet-rj.br)

Centro Federal de Educação Tecnológica Celso Suckow da Fonseca https://orcid.org/0000-0001-6656-9783

Maria A. G. Martinez

Centro Federal de Educação Tecnólogica Celso Suckow da Fonseca: Centro Federal de Educacao Tecnologica Celso Suckow da Fonseca

Research Article

Keywords: polarizer, modulator, graphene, multilayer structure, silicon photonics

Posted Date: April 16th, 2021

DOI: https://doi.org/10.21203/rs.3.rs-387266/v1

Version of Record: A version of this preprint was published at Optical and Quantum Electronics on August 6th, 2021. See the published version at https://doi.org/10.1007/s11082-021-03111-7.

Analysis of a tunable CMOS-compatible multilayer waveguide structure for dual polarizer-modulator operation

Renan S. Santos,[a,*] Maria A. G. Martinez[a]

[a]Centro Federal de Educação Tecnológica Celso Suckow da Fonseca, Photonics Lab, Electronic Engineering Department, Maracanã Avenue, 229 , Rio de Janeiro, Brazil, 20271-110

Abstract. A multilayer structure using graphene on a silicon waveguide is introduced and optimized to operate as a tunable TE-pass polarizer at 1310 nm or 1550 nm, a tunable TE/TM modulator at 1310 nm or 1550 nm, and a dual operation as a modulator at 1310 nm and a polarizer at 1550 nm. The analysis is based on the waveguide structure modal loss, the 2D graphene layer optical properties and its dependency on the applied chemical potential. The optimization is done by varying waveguide height and choosing the one with best figures of merit for each individual case and for the dual operation, the value that causes the least impairment overall is chosen. The polarizer tunability at 1310 nm or 1550 nm is attainable setting the applied chemical potential range from 0.55-0.65 eV or 0.45-0.55 eV, respectively. For the modulator tunability at 1310 nm or 1550 nm, the applied chemical potential range from 0.45-0.55 eV or 0.35-0.45 eV, respectively. The optimized waveguide silicon layer around 210 nm guarantees an extinction ratio better than 0.056 dB/µm for the polarizer and better than 0.045/0.133 dB/µm for the TE/TM modulator at 1310 nm, and better than 0.034 dB/µm for polarizer and better than 0.053/0.137 dB/µm for TE/TM modulator at 1550 nm. Further, the setting the chemical potential range at 0.45-0.55 eV, allows dual polarizer-modulator operation, with the modulator operating at 1310 nm and the polarizer operating at 1550 nm, presenting an extinction ratio better than 0.045 dB/µm and 0.034 dB/µm respectively. In all situations analyzed, insertion loss is lower than 0.007 dB/µm. The advantage of the structure in comparison with other similar devices relies in its versatility to operate as both modulator and polarizer, in different wavelengths, via a proper choosing of the applied chemical potential.

Keywords: polarizer, modulator, graphene, multilayer structure, silicon photonics.

***Renan S. Santos,** E-mail: renan.santos@aluno.cefet-rj.br

1 Introduction

In recent years, Silicon on Insulator (SOI) platforms has attracted much interest since it favors miniaturization of high-density Photonic Integrated Circuits (PICs) due to the strong confinement provided by the high refractive index difference between Silicon and the silica substrates (Azzam et al, 2014). Furthermore, SOI-based devices are usually compatible with Complementary Metal Oxide Semiconductor (CMOS) fabrication process, which allows manufacturing at lower costs than other typical semiconductors for optoelectronics, since it is a very mature fabrication technology.

Another material that has been drawing attention since its experimental discovery in 2004 (Novoselov et al, 2004) is graphene, which has been extensively studied for applications in several fields, given its unique properties, among which, its high thermal

conductivity (10 times higher than copper) and its high mechanical resistance (Nguyen and Zhao, 2014). In optoelectronics, graphene, in function of its properties like high electronic mobility (250 times higher than silicon), high electrical conductivity (35% higher than copper) and high transparency in the visible spectrum (around 97%) (de Oliveira and de Matos, 2015; Liu, Yin and Ulin-Avila, 2011), appears as a suitable choice of material for use in integrated optics devices, where its reduced thickness (0.34 nm for a single graphene layer) provide it additional advantage over other materials since it allows the development of integrated optic devices without significantly increasing footprint (Vakil and Engheta, 2011; Novoselov, Fal'ko and Colombo, 2012).

Several research papers combine a SOI platform with graphene in order to devise some devices like modulators, polarizers, and so on (de Oliveira and de Matos, 2015; Liu, Yin and Ulin-Avila, 2011; Vakil and Engheta, 2011; Hao et al, 2015; Gosciniak and Tan, 2013; Mohsin et al, 2014; Santos, Martinez and Giraldi, 2018).

In (He and Liu, 2017), He and Liu proposed a broadband polarizer based on a graphene-coated surface silicon-core microfiber in an elliptical silica cladding, achieving extinction ratios of the order of 30 dB, with a graphene length of 1.5 mm, where the TE or TM-pass behavior can be tuned by adjusting the core radius of the silicon-core. In (de Oliveira and de Matos, 2015), de Oliveira and de Matos showed how waveguide design plays an essential role in graphene devices characteristics, by simulating a rib waveguide structure with different dimensions and superstrates. The device can operate as a TE-pass or TM-pass polarizer depending on the superstrate. In (Hao et al, 2015), Hao et al. proposed a TE/TM independent polarizer based on Mach-Zehnder interferometer, whereby coating the interferometer arms with graphene, on top, bottom and lateral sides, the chemical potential dependence of graphene's permittivity can be explored by applying a voltage on top and bottom layers or on lateral layers, changing electric field component

losses, thus leading to TE or TM-pass behavior. The achieved extinction ratio is on the order of 20 dB, with the device length of some tens of μm. In (Yin et al, 2015), Yin et al propose an ultra-compact TE-pass polarizer with multilayer graphene embedded in a silicon slot waveguide, based on graphene epsilon-near-zero effect, with an extinction ratio as high as 4.5 dB/ μm and an insertion loss of only 0.01 dB/μm. In (Zhang et al, 2016), Zhang et al have shown a polarization beam splitter utilizing a graphene-based asymmetrical directional coupler combining a silicon waveguide and a graphene multilayer embedded silicon waveguide, obtaining extinction ratios of 18.2 dB and 21.2 dB and insertion losses of 0.16 and 0.36 dB for the thru and cross ports, respectively. In (Yin et al, 2016), Yin et al have shown a TE-pass polarizer using a cascade of multiple few-layer graphene embedded silicon waveguides, where graphene's epsilon-near-zero effect is used to attenuate the TM mode more than TE mode, obtaining an extinction ratio of 20 dB for an insertion loss lower than 0.13 dB.

In (Liu, Yin and Ulin-Avila, 2011), Liu et al. demonstrated a broadband, graphene-based electroabsorption optical modulator using a silicon-core waveguide coated with a graphene layer separated by a thin alumina spacer. The device performance is similar to that of traditional semiconductor materials, with the advantage of small footprint and easy integration of graphene to novel optoelectronic materials. The modulation depth of 0.1 dB/ μm is achieved with a device footprint under 25 $\mu m^{2.}$ In (Gosciniak and Tan, 2013), Gosciniak, and Tan investigated theoretically the behavior of a graphene electroabsorption modulator based on a silicon ridge waveguide with two graphene sheets separated by a spacer, with simulations being realized for several configurations of the ridge, concluding that the modulator can be significantly optimized by choosing appropriate dimensions, and achieving 3 dB modulation with a device length of 600 nm, power consumption as low as 1 fJ/bit and a figure of merit (Extinction

Ratio/Insertion Loss) as high as 220. In (Mohsin et al, 2014), Mohsin et al. demonstrated a graphene-based SOI electro-absorption modulator with insertion loss as low as 3.3 dB, while achieving an extinction ratio of 16 dB. In (Hu and Wang, 2017), Hu and Wang demonstrated a high figure of merit graphene modulator based on plasmonic slot waveguide, evaluating the device for different materials and geometries. The optimized device proposed has an extinction ratio of 8.257 dB/ μm and an insertion loss of 0.0376 dB/ μm, which leads to an overall figure of merit of 218. The device also has a power consumption as low as 0.008 fJ/bit.

Overall, graphene-based waveguide structures are highly optimized for operation either as a modulator or polarizer at a specific wavelength. Nevertheless, many optical systems use multiple wavelengths. Thus, more versatile approaches to waveguide structures for optical systems are needed. In this work, a single SOI-based, CMOS compatible multilayer waveguide structure is analyzed and optimized to operate as: (i) a TE-pass polarizer tunable to operate at 1310 nm or 1550 nm; (ii) an modulator tunable to operate at 1310 nm or 1550 nm; (iii) either a modulator or a TE-pass polarizer to operate either at 1310 nm or 1550 nm, respectively. The analysis is done by simulating the behavior of the waveguide regarding the applied chemical potential as well as waveguide height for both wavelengths. The structure is evaluated via figures of merit such as the Extinction Ratio and Insertion Loss. It can be shown that the structure versatility relies in a proper choice of graphene chemical potential range, multilayer waveguide structure design parameters and selective modal losses.

The CMOS compatible multilayer waveguide structure is presented in section 2, along with the modeling approach used in the analysis. Section 3 show the results obtained for the polarizer, modulator and dual-mode operations, as well as considerations

about the optimal dimensions for each case. In Section 4, conclusions of the work are presented.

2 Multilayer waveguide structure and graphene modeling

In (Santos, Martinez and Giraldi, 2018), we reported on the performance of a CMOS compatible multilayer structure, composed by a silica substrate, a silicon core, a graphene layer and an alumina superstrate, as a tunable TE-pass polarizer with a 6dB/cm extinction ratio over a 600 nm band. In this work, the proposed reduced dimensionality multilayer structure is redesigned as a rib waveguide, to operate as a tunable TE-pass polarizer at 1310 nm or 1550 nm wavelengths, as shown in Figure 1. The design is based on the structure presented in (Liu, Yin and Ulin-Avila, 2011), with the electrodes placed more than 500 nm away from the waveguide core in order to minimize the electrode influence on the field.

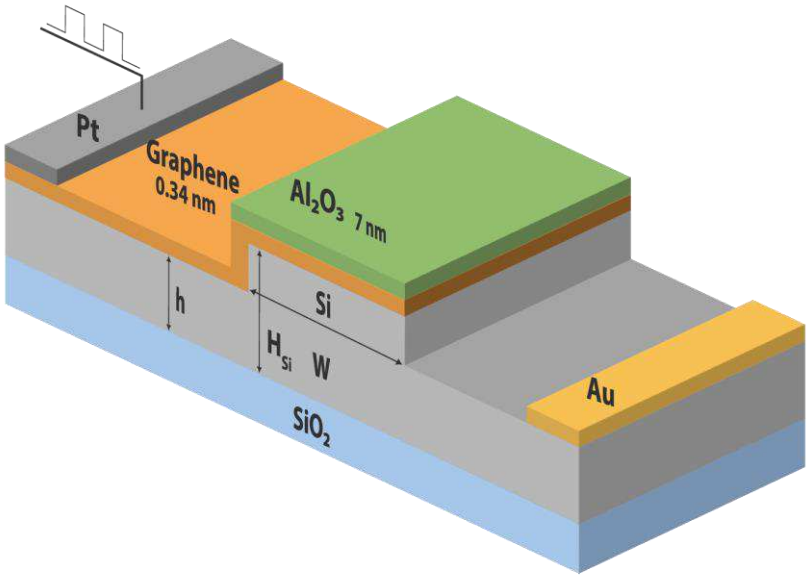

Figure 1: Rib waveguide used for analysis. W = 900 nm and h = 150 nm

The structure modal losses are accounted by applying Effective Index Method (Okamotto, 2006; Kawano and Kitoh, 2001; Marcatili, 1974; Ramaswamy, 1974) for

finding the effective index in both confinement directions separately and solving Maxwell´s equations and applying boundary conditions to the tangential and electric and magnetic fields components for TE and TM modes. The complex effective index n_{eff} is defined as $n_{eff} = \gamma/k_0 = (\beta + j\alpha)/k_0$ and is a function of the wavelength dependent materials refractive indexes and layers thicknesses. γ is the complex propagation constant, α is the absorption coefficient, β is the phase constant, and k_0 is the free space wave number.

The graphene layer is treated as an isotropic material (Kim, Kim and Kim, 2019; Xiao et al, 2018; Yin et al, 2015; Zhang et al, 2016), and its electrical an optical properties are modeled (de Oliveira e de Matos, 2015; Vakil and Engheta, 2011; Hao et al, 2015; He and Liu, 2017; Kim, Kim and Kim, 2019) by Kubo's formula, that takes into account the inter and intraband transitions contribution to 2D graphene conductivity (Hanson, 2008), given by:

$$\sigma_{intra}(\omega, \mu_c, T, \Gamma) = -j\frac{e^2 k_b T}{\pi\hbar^2(\omega - j2\Gamma)}\left(\frac{\mu_c}{k_b T} + 2ln\left(e^{-\frac{\mu_c}{k_b T}} + 1\right)\right) \quad (1)$$

$$\sigma_{inter}(\omega, \mu_c, \Gamma) = -j\frac{e^2}{4\hbar\pi} ln\frac{2|\mu_c| - (\omega - j2\Gamma)\hbar}{2|\mu_c| + (\omega - j2\Gamma)\hbar} \quad (2)$$

where e is electron charge, $\hbar$ is Planck's reduced constant, ω is angular frequency. μ_c is the chemical potential, which is defined by $\boldsymbol{\mu_c = \mu_v + \mu_{cp}}$, where $\boldsymbol{\mu_v}$ is the applied chemical potential and $\boldsymbol{\mu_{cp}}$ is the chemical potential change caused by to charge puddles and topographic corrugations that appears when graphene is deposited on a dielectric substrate (Zhang et al, 2009; Lewkowicz and Rosenstein, 2009). k_b is Boltzmann constant, T is the temperature and Γ is the scattering parameter, which is linked to carrier relaxation time (τ) by $\Gamma = \frac{\hbar}{\tau}$. In this work, we consider $\Gamma = 5$ meV, as referenced in

literature as a reasonable estimate of scattering parameter for graphene (Lu and Zhao, 2012; Kuzmenko et al, 2008). Graphene's refractive index is defined as relative permittivity is defined as (Xu et al, 2015) $n_g = \sqrt{1 - \frac{j\sigma}{\omega\varepsilon_0\delta_g}}$, where δ_g is the graphene layer thickness, and $\sigma = \sigma_{intra} + \sigma_{inter}$.

Graphene's chemical potential is typically changed via an applied voltage, in a capacitive arrangement where at least one of the electrodes is in contact with graphene, changing carrier density in graphene (and thus, the chemical potential) according to the applied voltage (Liu, Yin and Ulin-Avila, 2011; Hao et al, 2015; Gosciniak and Tan, 2013; Mohsin et al, 2014).

3 Results and discussion

The rib waveguide losses (in dB/μm), defined as $20log_{10}e^{-k_0 Im(n_{eff})}$, for wavelength given in μm, for both fundamental TE and TM modes as a function of wavelength for four different values of chemical potential, and waveguide structure height, H_{Si}, equal to 230 nm , are shown in Figure 2.

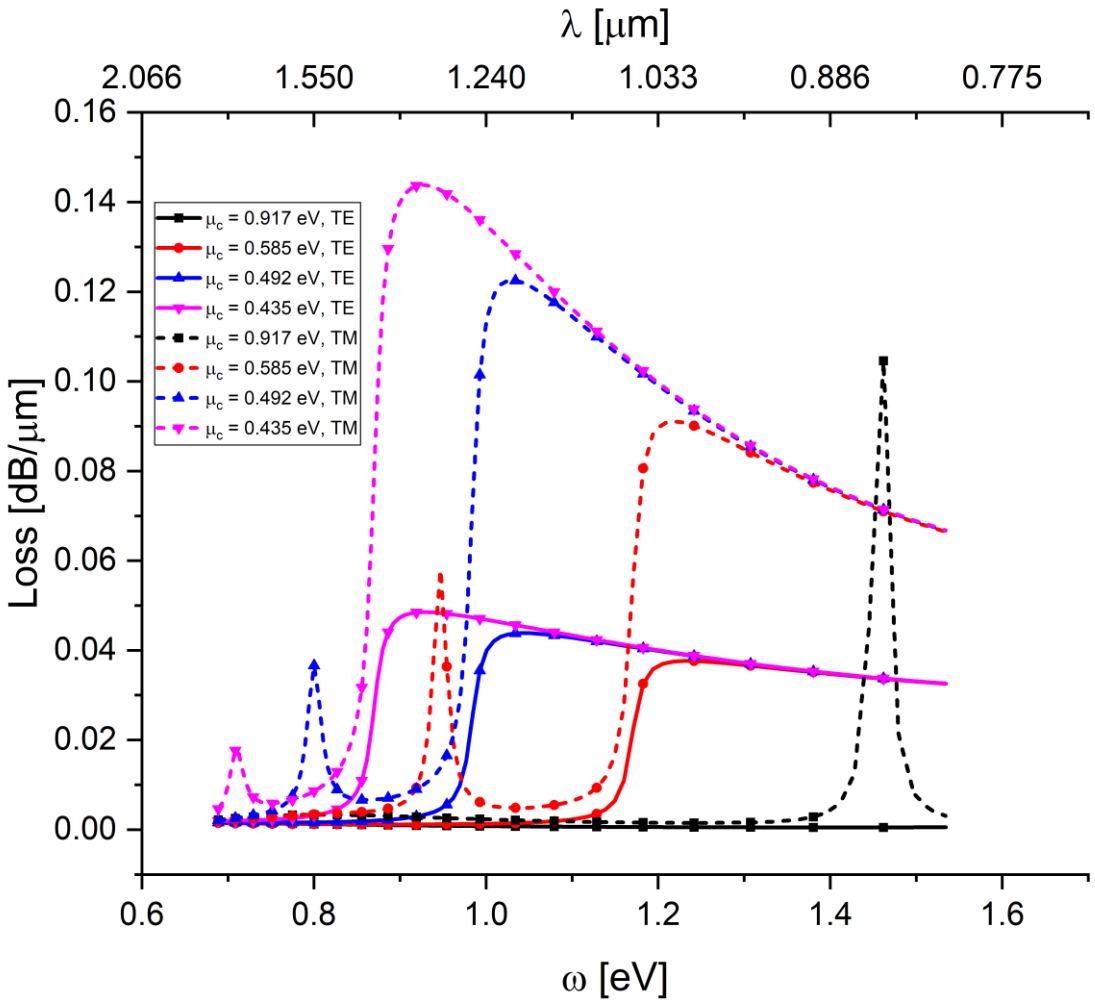

Figure 2: Losses (in dB/μm) as a function of wavelength , and correspondent value in eV, for the fundamental TE mode (solid lines) and TM mode (doted lines), for the chemical potentials of 0.435 eV (inverted triangle), 0.492 eV (triangle), 0.585 eV (circle) and 0.917 eV.(square)

The structure behaves differently for the TE and TM modes. It can be seen that there are resonant-like peak losses for TM modes around the frequencies of 0.7, 0.8, 0.95 and 1.5 eV, for the chemical potentials of 0.435, 0.492, 0.585 and 0.917 eV, respectively, which are nonexistent for the TE modes. The chemical potentials were chosen due to the appearance of these losses at the wavelengths of 1.8, 1.55, 1.31 and 0.8 μm, corresponding to the end of the analyzed range, the wavelengths of interest and the beginning of analyzed range, respectively. These tunable and highly selective losses for TM mode occur at the wavelengths where graphene permittivity is near zero (de Oliveira and de Matos, 2015; Mahmoud and Engheta, 2014; Ziolkowski, 2004), as shown in

Figure 3. As graphene permittivity approaches zero, the fraction of the structure electric field normal (E_x) to the core-graphene interface, increases within the graphene layer, leading to the highly selective losses. As normal electric field component is only present for TM modes, consequently the near zero effects do not affect TE modes. The inset of the Figure 3, the near-zero region is highlighted, showing that, for higher values of chemical potential, graphene's permittivity is closer to zero, leading to higher losses.

In Figure 2, other losses, not as selective as those mentioned above, but tunable as well, exist for TE and TM modes around 0.9, 1.05 and 1.2 eV, for chemical potentials values of 0.435, 0.492 and 0.585 eV, respectively. Differently from the resonant-like ones, these losses decrease with chemical potential, but also affect more intensely the TM mode. This wavelength dependent losses behavior follows the real part of graphene's refractive index, e.g., it increases with wavelength, getting even higher than silicon's and, after this point, decreases, as shown in Figure 4.

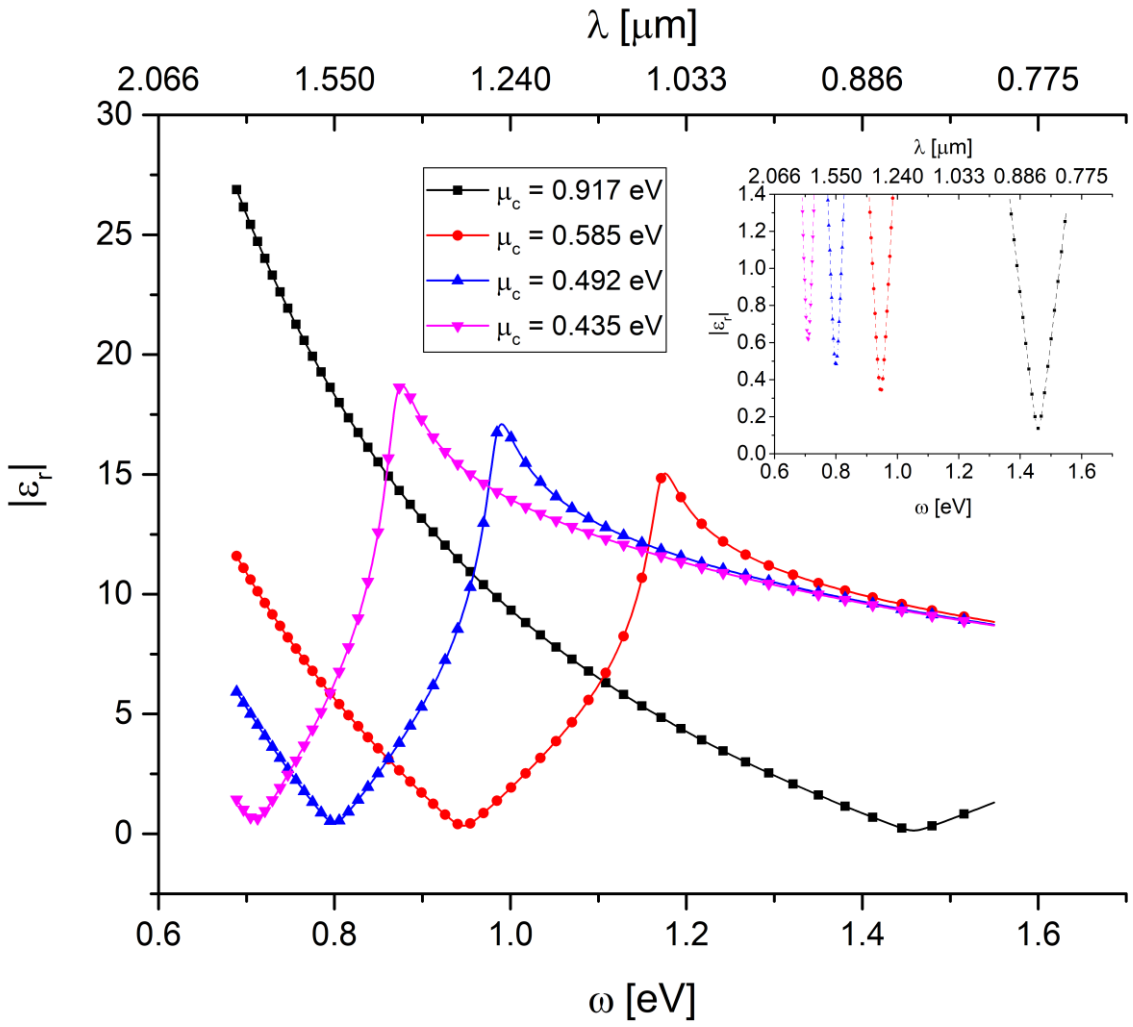

Figure 3: Absolute value of graphene permittivity as a function of wavelength, for the chemical potentials of 0.435 eV, 0.492 eV, 0.585 eV and 0.917 eV. Inset: magnification of epsilon near-zero region.

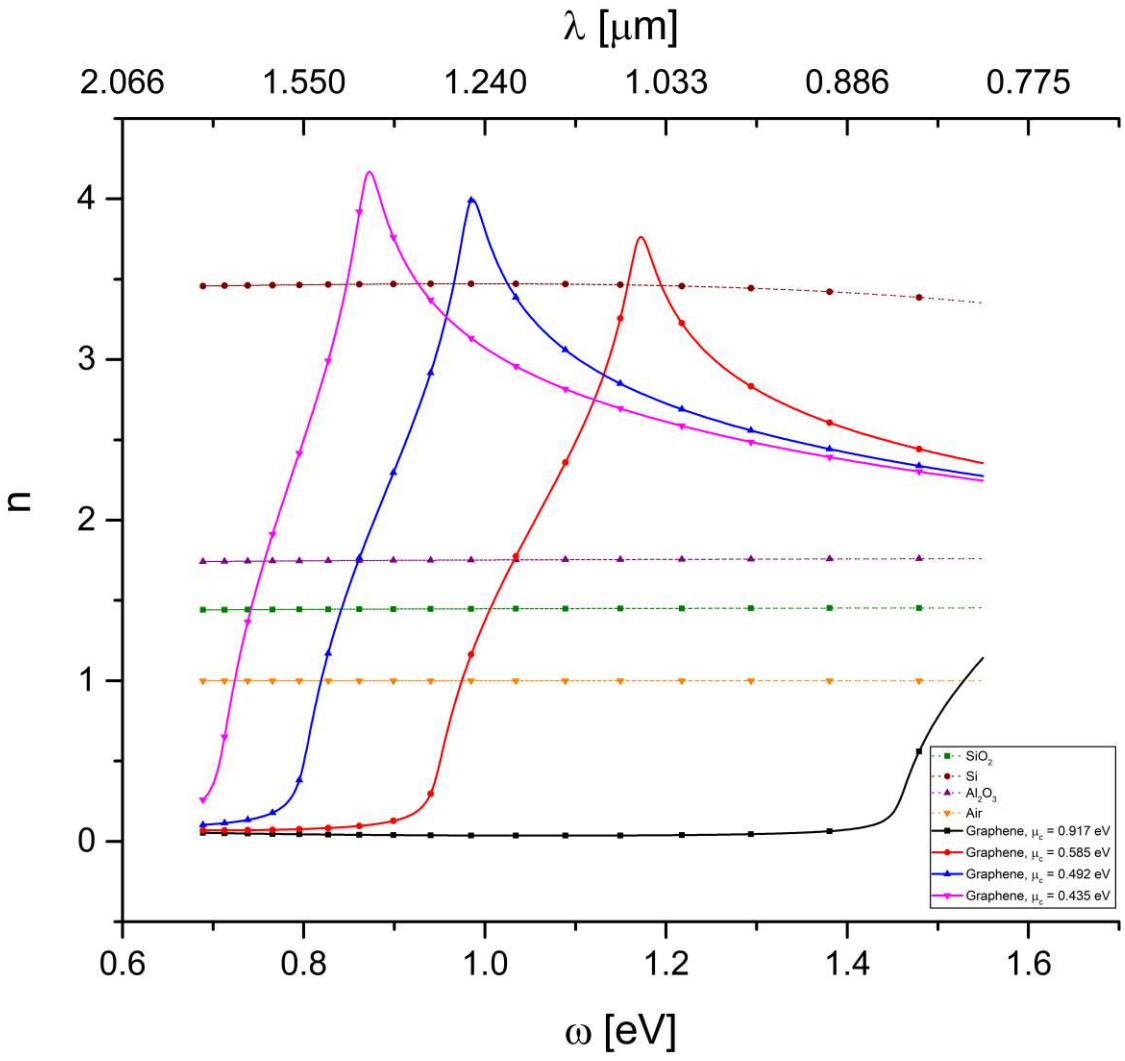

Figure 4: Real part of graphene refractive index (solid lines) as a function of wavelength, for the chemical potentials of 0.435 eV (inverted triangle) , 0.492 eV (triangle), 0.585 eV (circle) and 0.917 eV (square) , and the refractive SiO_2 (dotted line-square), Si (dotted line-circle) and Al_2O_3 (dotted line-triangle) layers.

3.1 A tunable TE-pass polarizer to operate at 1310 or 1550 nm

The multilayers structure can operate as a tunable TE-pass polarizer at 1310 nm or 1550 nm, if the chemical potential values of 0.585 eV or 0.492 eV are selected, respectively. Graphene's chemical potential is typically changed via an applied voltage, in a capacitive arrangement where at least one of the electrodes is in contact with graphene, changing carrier density in graphene (and thus, the chemical potential) according to the applied voltage (Liu, Yin and Ulin-Avila, 2011; Hao et al, 2015; Gosciniak and Tan, 2013; Mohsin et al, 2014).

The waveguide core height impact on the tunable TE-pass polarizer performance is analyzed. In Figure 5, the calculated losses , for TE and TM modes as a function of silicon waveguide core height is shown, for 1310nm and 1550 nm wavelengths.

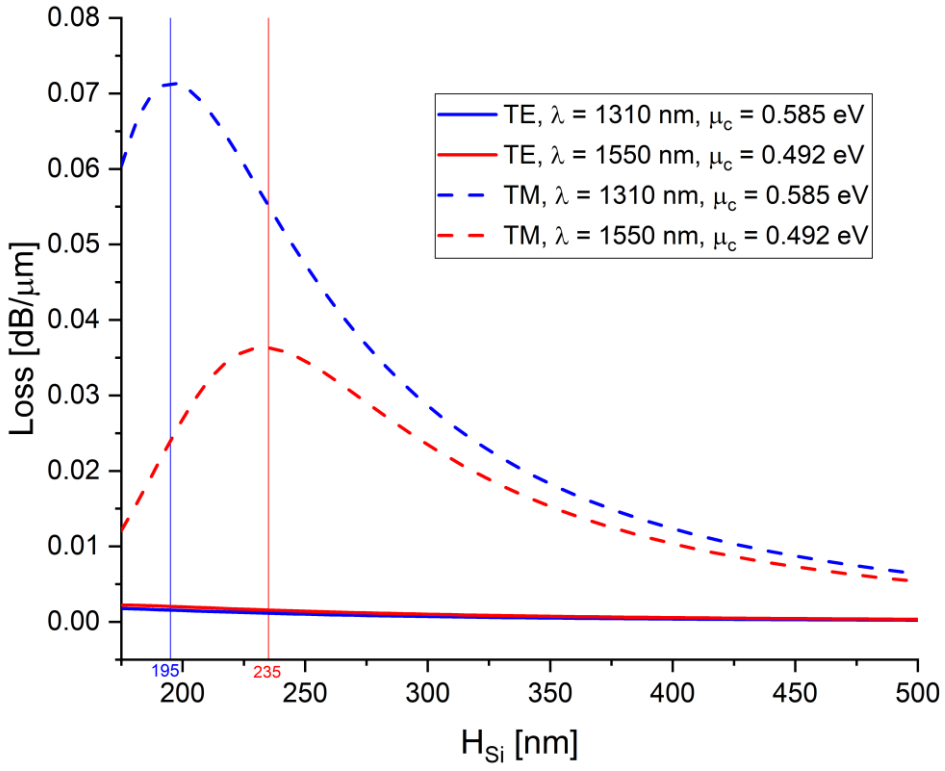

Figure 5: TE (solid line) and TM (dotted lines) modes normalized absorption coefficient as a function of silicone core height for λ = 1310 nm and λ = 1510 nm.

In Figure 5, we observe that the silicon core height, which maximizes losses for TM mode is around 195 nm for 1310 nm wavelength and 235 nm for 1550 nm wavelength. Nonetheless, in order to further elucidate the operation of the structure as a polarizer, it is important to observe the figure of merit of the structure for this mode of operation (Extinction Ratio/Insertion Loss – ER/IL), which is shown in Figure 6. Extinction ratio for the polarizer is defined as the difference between TM and TE mode losses ($ER = L_{TE} - L_{TM}$) and insertion loss is defined as the losses for TE mode ($IL = L_{TE}$). It is shown that the silicon core heights which effectively optimize the use of the

structure as a polarizer are around 215 nm (for 1310 nm) and 260 nm (for 1550 nm), respectively.

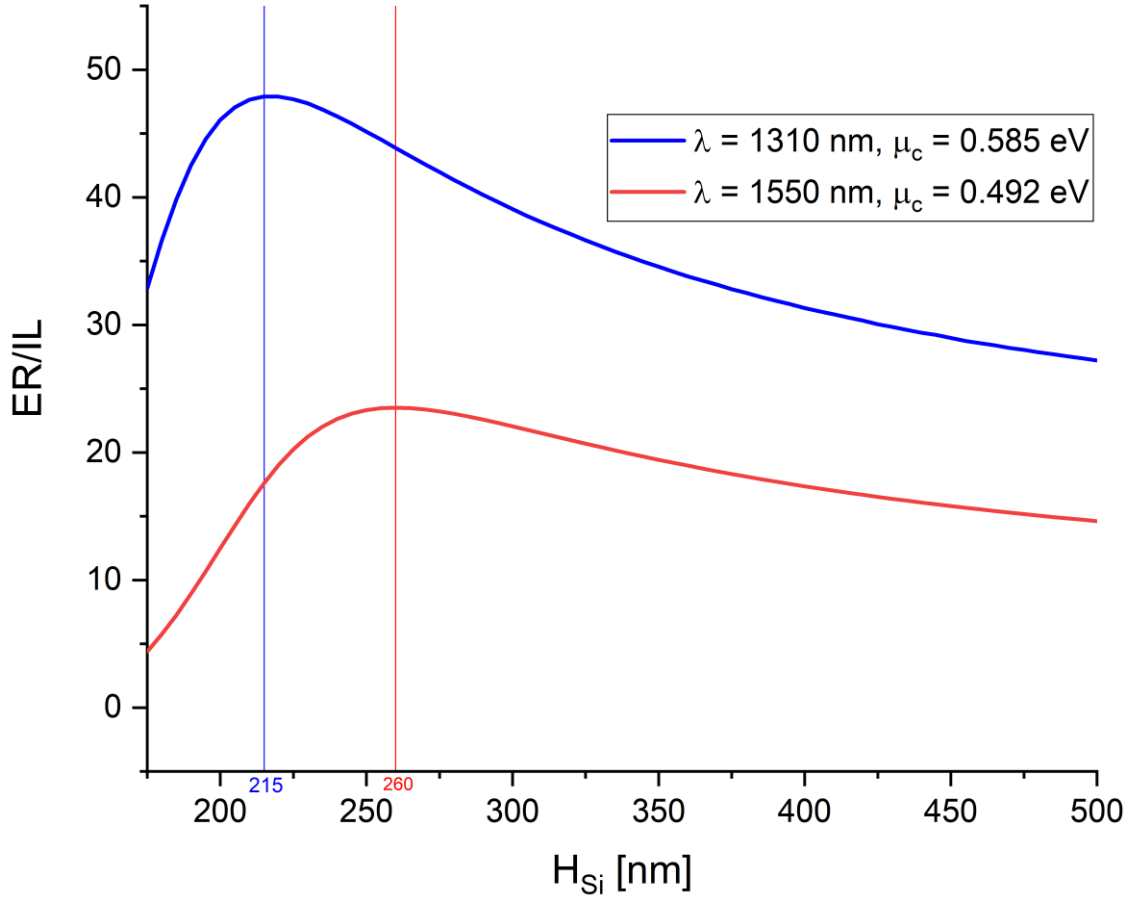

Figure 6: Figure of merit as a function of silicon core height for λ = 1310 nm and λ = 1510 nm.

There is a clear difference in the figure of merit between the 1550 nm and 1310 nm wavelengths, being it higher (around 100% higher) for the 1310 nm wavelength. If we observe Figure 3 again, we perceive that this difference is because the epsilon near-zero effect is more pronounced at the chemical potential of 0.585 eV (corresponding to the 1310 nm wavelength) in comparison to the chemical potential of 0.492 eV (corresponding to the wavelength of 1550 nm). Table 1 summarizes the polarizer figures of merit for the optimized core layer height at each wavelength, for the single structure (H_{si}=260 nm) to operate at both wavelengths. It can be noticed that, for the single

structure, the performance penalty in comparison to the optimized case for 1310 nm is only 8.3%.

Table 1 Figure of merit, considering the operation as a polarizer, for the optimized and single structure, at the 1310 nm and 1550 nm wavelengths

	Optimized Structure		**Single Structure**	
λ (nm)	1310	1550	1310	1550
H_{Si} (nm)	215	260	260	
ER(dB/μm)	0.0644	0.0312	0.0418	0.0312
IL (dB/μm)	0.0013	0.0013	0.000952	0.0013
FOM	≅48	≅23.5	≅44	≅23.5

3.2 A tunable modulator to operate at 1310 or 1550 nm

The multilayer structure can also operate as a tunable modulator at 1310nm or 1550nm. For instance, for operation at 1310 nm or 1550nm, we set the chemical potential within the 0.450-0.550 eV or 0.350-0.450 eV ranges, respectively. Although the use of lower chemical potentials can enhance the extinction ratio of the structure, operation for much lower chemical potentials impairs the dual modulator-polarizer operation intended, as the chemical potential ranges used would fall way below the polarizer chemical potential ranges. The structure normalized absorption coefficient as a function of core waveguide height for the two operating conditions are shown in Figures 7 and 8.

For the TE mode, Figures 7 (a) and 8 (a), the best modulation depth, e.g., the higher contrast between the maximum and minimum absorption coefficients in the chemical potential range occurs around 200 nm (for 1310 nm) and 190 nm (for 1550 nm). Nevertheless, for TM mode, as shown in Figures 7 (b) and 8 (b), the width which optimizes the operation as a modulator is around 210 nm (for 1310 nm) and 220 nm (for 1550 nm).

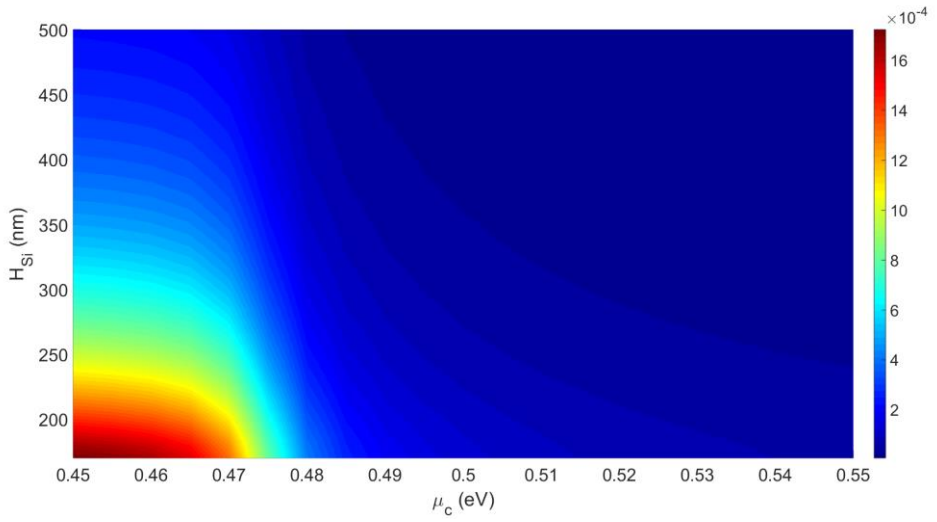

(a)

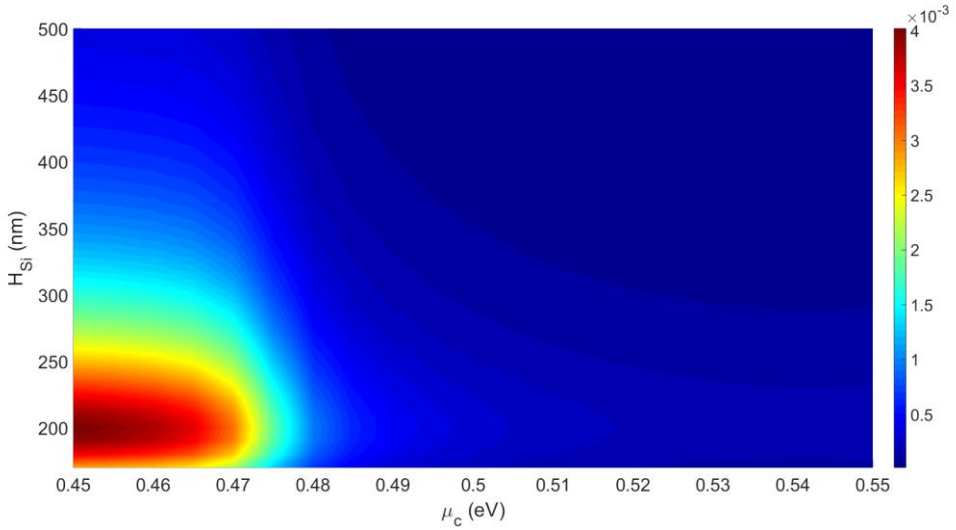

(b)

Figure 7: Normalized absorption coefficient as a function of silicon core height and chemical potential for λ = 1310 nm nm. (a) TE mode (b) TM mode

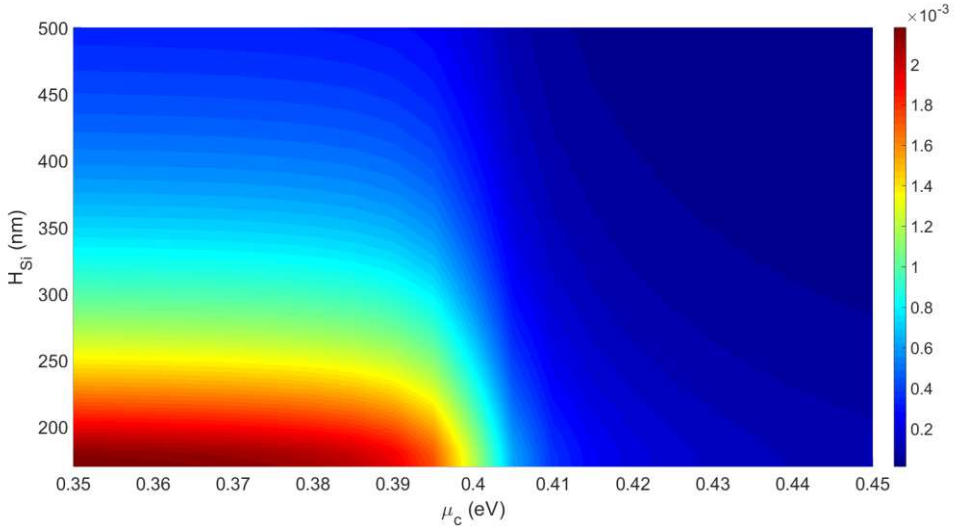

(a)

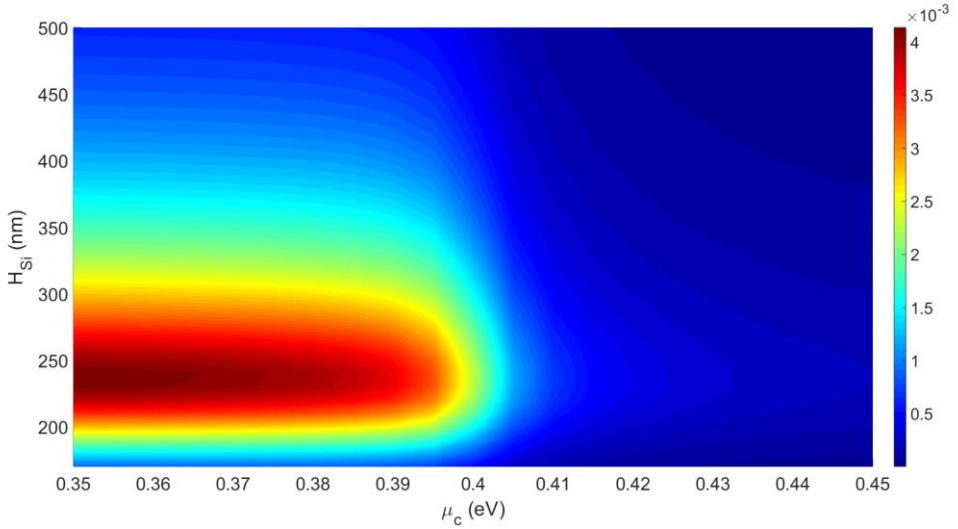

(b)

Figure 8: Normalized absorption coefficient as a function of silicon core height and chemical potential for λ = 1550 nm. (a) TE mode (b) TM mode

In Figures 9 and 10, the normalized absorption as a function chemical potential, for the two ranges values for tunable operation, are shown for the TE and TM modes, for three different core waveguides heights (including the optimized ones), respectively. For TE mode, the increase in height decreases extinction ratio, and extinction ratios of 0.0695 dB/μm and 0.0734 dB/μm are achieved for 1310 nm and 1550 nm wavelengths, respectively. For TM mode, this the values for extinction ratio are around 0.16 dB/μm and 0.14 dB/μm for the wavelengths of 1310 and 1550 nm, respectively.

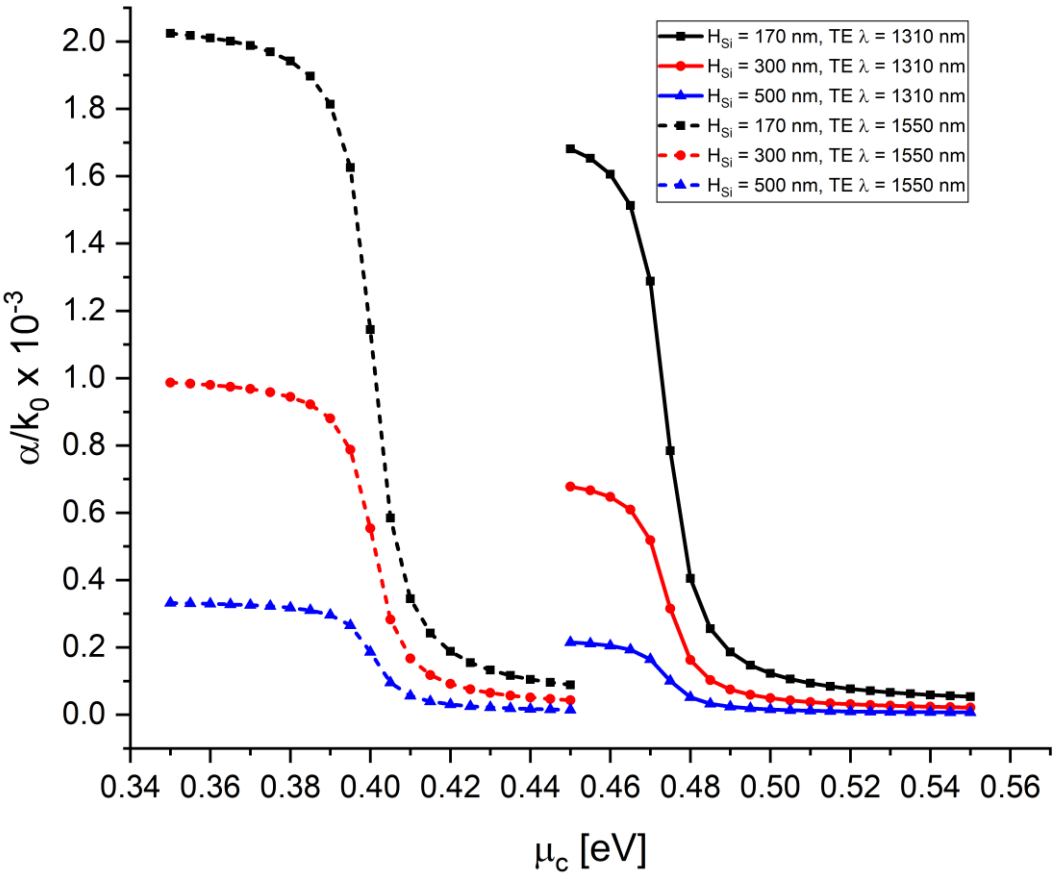

Figure 9: Normalized absorption coefficient as a function of chemical potential, for TE modes, for three different values of silicon core height, at λ = 1310 nm and λ = 1550 nm wavelength

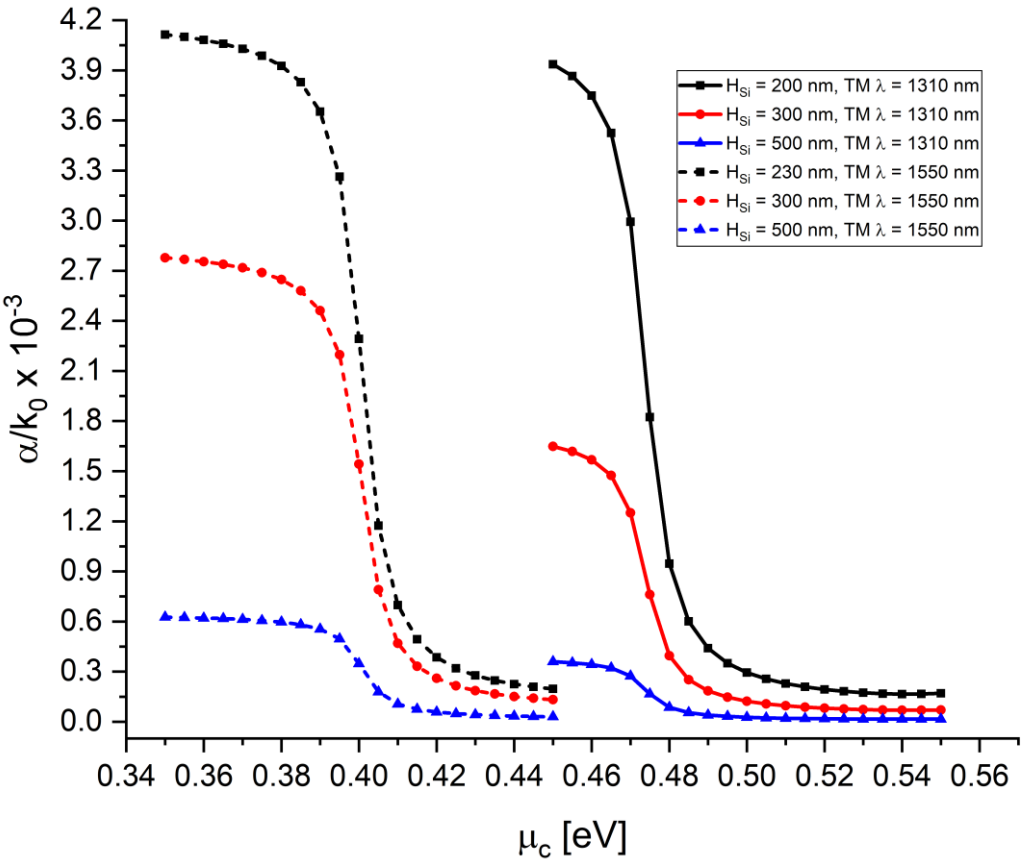

Figure 10: Normalized absorption coefficient as a function of chemical potential, for TM modes, for three different values of silicon core height, at λ = 1310 nm and λ = 1550 nm wavelength

Table 2 summarizes the ER and IL values for the heights of silicon core, which maximizes ER for TE and TM modes at the 1310 and 1550 nm wavelengths. Extinction Ratio for the modulator is defined as the difference between maximum and minimum losses in the range of chemical potentials analyzed, and insertion loss is defined as the minimum loss. We notice that when the structure is optimized, the figures of merit are better for TE mode (27% higher than TM mode for 1310 nm and 10% higher for 1550 nm). A single structure to operate at both wavelengths is set to waveguide structure height for the 1310 nm, TM mode, which guarantees the performance for the worst case analyzed. The figures of merit, considering a single structure capable of operating as a modulator at both wavelengths, are also depicted. It is also noticeable that for the single structure, the overall figure of merit changes only slightly compared to the optimized

structures.

Table 2 Figures of merit, considering the operation as a modulator for the optimized and single structure, at the 1310 nm and 1550 nm wavelengths.

	Optimized Structure				Single Structure			
λ (nm)	1310		1550		1310		1550	
Mode	TE	TM	TE	TM	TE	TM	TE	TM
H_{Si} (nm)	170	200	170	230	230			
ER(dB/μm)	0.0695	0.1602	0.0734	0.1378	0.0457	0.1331	0.0531	0.1378
IL (dB/μm)	0.0023	0.0072	0.0034	0.0069	0.0015	0.0060	0.0024	0.0069
FOM	≅30	≅22	≅22	≅20	≅30	≅22	≅22	≅20

3.3 Modulator operating at 1310nm and TE-pass polarizer operating at 1550 nm

In previous sections, we analyzed the structure operation as a tunable polarizer and a modulator at different wavelengths. The selection of the operation as a modulator or polarizer is selected by a proper choice of chemical potential. For instance, for the 1310 nm wavelength, the structure works as a TE-pass polarizer at 0.585 eV chemical potential and as a TE/TM modulator at the chemical potential range between 0.45 and 0.55 eV. For the 1550 nm wavelength, the structure works as TE-pass polarizer at 0.492 eV chemical potential and as a TE/TM modulator at the chemical potential range between 0.35 and 0.45 eV. Additionally, the structure can be operated in both modes (modulator and polarizer), at the same range of chemical potential in different wavelengths, as shown in Table 3.

Table 3 Modes of operation for the structure, according to chemical potential, for different wavelengths

		Chemical potential range (eV)		
		0.35 – 0.45	0.45 – 0.55	0.55 – 0.65
Wavelength	1310nm	X	Modulator	Polarizer
	1550nm	Modulator	Polarizer	X

The figures of merit for a single structure, dual modulator/polarizer operation are shown in Table 4, for a silicon core height of 230 nm. By using the 230 nm height, we

notice that the performance (figure of merit) as a polarizer is around 11% lower for 1550 nm wavelength and less than 1% lower for 1310 nm wavelength when compared to the 260 nm height (see Table 1). Thus, the performance penalty in for the single structure when compared to the optimized cases presented is around 11% (worst case is from 23.5 to 21 for the polarizer operation at 1550nm).

Table 4 Summary of the figures of merit, considering both modes of operation (modulator and polarizer), for the proposed structure at the 1310 nm and 1550 nm wavelengths

	TE-Pass Polarizer		**Modulator**			
λ (nm)	1310	1550	1310		1550	
μ_c (eV)	0.55 – 0.65	0.45 – 0.55	0.45 – 0.55		0.35 – 0.45	
Mode	----------		TE	TM	TE	TM
H_{Si} (nm)			230			
ER(dB/μm)	0.0567	0.0346	0.0457	0.1331	0.0531	0.1378
IL (dB/μm)	0.0012	0.0016	0.0015	0.0060	0.0024	0.0069
FOM	≅47	≅21	≅30	≅22	≅22	≅20

Another important detail lies in the operation bandwidth of the device. Considering the values for device resistance and capacitance presented in (Liu, Yin and Ulin-Avila, 2011) as 600 Ω and 0.22 pF, respectively, the frequency response of the device, based on the RC model of the device is shown in Figure 11. The estimate modulation speed is around 2 GHz.

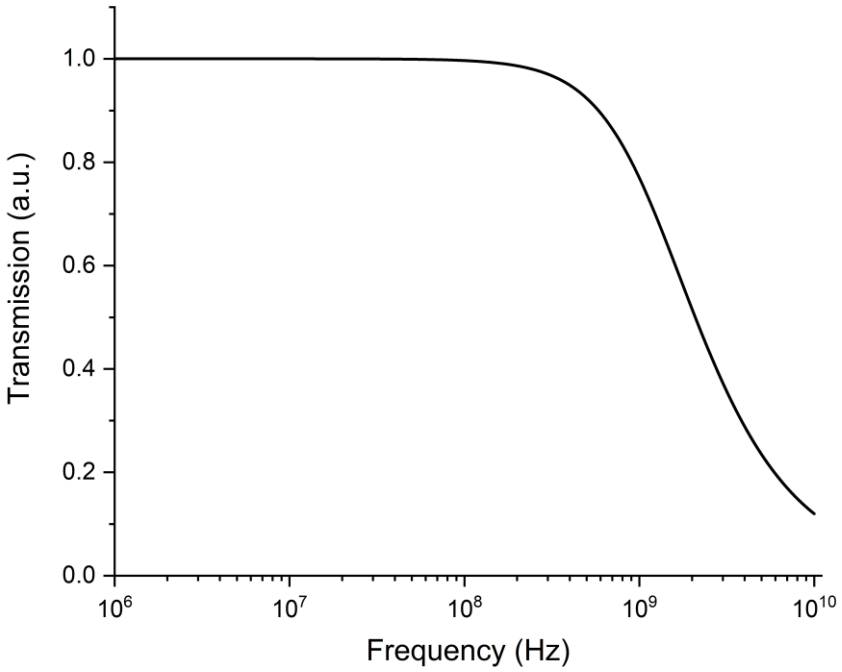

Figure 11: Estimated frequency response of the structure

In order to make it easier to compare the proposed structure with others in literature, Tables 5 and 6 summarize the main parameters, considering the 1550 nm wavelength and TE mode for the modulator.

Table 5 Comparison of the parameters of the proposed structure with selected works from the literature for the TE-pass polarizer operation

	TE-Pass Polarizer			
	This Work	He and Liu	De Oliveira and de Matos	Yin et al
ER (dB/μm)	0.0346	0.021	0.006	4.47
IL (dB/μm)	0.0016	-	0.02979	0.2
Wavelength range	0.85 – 1.71	0.7 – 1.7	-	1.546 – 1.599

Table 6 Comparison of the parameters of the proposed structure with selected works from the literature for the modulator operation

	Modulator			
	This work	Liu et al	Gosciniak and Tan	Hu and Wang
ER (dB/μm)	0.0531	0.1	0.29	8.257
IL (dB/μm)	0.0024	-	0.023	0.0376
Wavelength range	0.85 -1.71	1.35 – 1.6	-	1.26 – 1.93
Modulation Speed	2 GHz (est.)	1.2 GHz	0.5 THz	-

Overall, the figures of merit of the proposed structure are on par with other selected works from the literature. Figures of merit much lower than the ones in literature, particularly when this work is compared to (Yin et al, 2015) in the case of the TE-pass polarizer and (Hu and Wang, 2017) for the modulator must be treated with caution, since these designs are more complex and highly optimized for the proposed polarizer or modulator operation. (Yin et al, 2015) shows an ultra-compact TE-pass polarizer with multilayer graphene embedded in a silicon slot waveguide and (Hu and Wang, 2017) demonstrate a graphene modulator based on plasmonic slot waveguide. Besides being more complex than the structure presented in this work, none of the designs in literature shows the possibility to operate as a dual polarizer-modulator structure as shown in this work.

Lastly, both polarizer and modulator characteristics can be further elucidated by observing the field intensity distribution for both polarizer and modulator operation, as shown in figures 12 and 13.

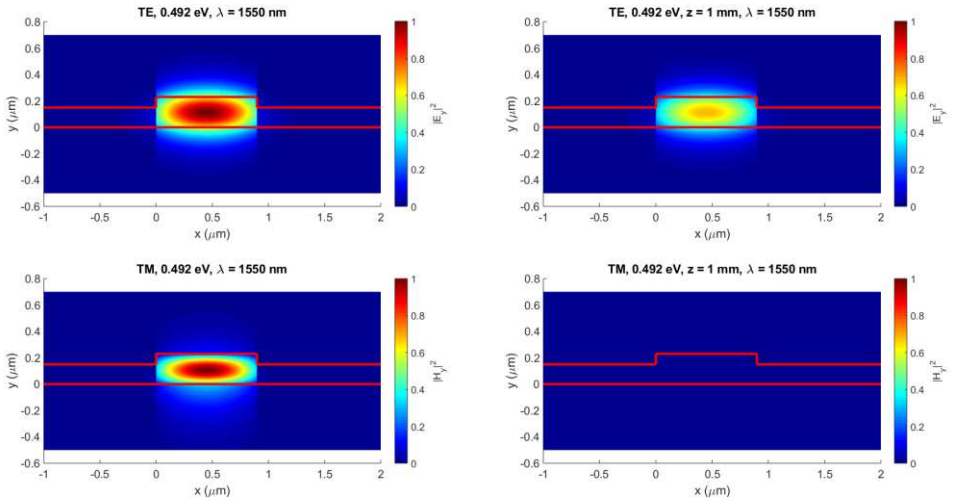

Figure 12: Field intensity for TE (upper row) and TM (lower row) modes for polarizer operation, at the beginning of the waveguide (first column) and after 1 mm (second column) for 1550 nm and 0.492 eV chemical potential

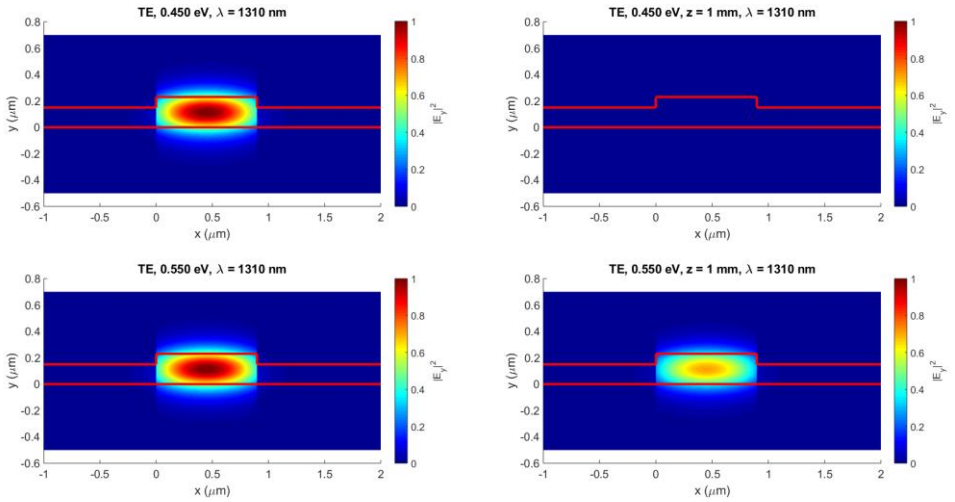

Figure 13: Field intensity for TE mode for modulator operation, at the beginning of the waveguide (first column) and after 1 mm (second column) at 0.450 eV (upper row) and 0.550 eV (lower row) for 1310 nm

Regarding the polarizer operation, observing figure 11, it is clear how the TM mode suffers stronger attenuation in the waveguide than the TE mode. TE mode loses around 35% of its intensity after 1 mm, as TM mode loses more than 90%.

As for the modulator, it can be seen in figure 12 that the field intensity decays more than 90% after 1 mm for the 0.45 eV chemical potential at 1310 nm. Nevertheless, it decays only around 35% for 0.55 eV, at the aforementioned wavelength.

4 Conclusion

We analyzed the performance of SOI based, CMOS compatible rib waveguide single structure as a TE-pass polarizer tunable to operate at 1310nm or 1550nm, a modulator tunable to operate at 1310nm or 1550nm, and a TE-pass polarizer to operate at 1550nm and a modulator to operate at 1310nm. We optimized the height of the waveguide core and show that the structure is capable of operating in both wavelengths as a polarizer via a suitable choice of chemical potential, and with penalties as low as 8.3%, when compared to the optimized height for each wavelength (ER/IL of 48 for the dual-wavelength structure versus 44 for the optimized height for 1310 nm). Also, in another chemical potential range, it can be used as a modulator, for both TE and TM modes and both

wavelengths with a change in the figure of merit lower than 1% when compared to the optimized height cases (ER/IL higher than 20 in all cases). Further, the waveguide multilayer structure allows simultaneous operation as a modulator at 1310 nm and a polarizer at 1550 nm via the tuning of chemical potential with a penalty in figure of around 11% when compared to the optimized height cases (ER/IL of 21 compared to 23.5 for the optimized case of the polarizer for 1550 nm). Extinction ratio for the dual structure are on the order of 0.05 dB/μm for the polarizer operation, which is on par with some of the reported devices in literature (He and Liu, 2017), although lower than some devices based on structures such as Mach-Zehnder interferometer or slot waveguides (Hao et al, 2015; He and Liu, 2017). For the modulator, extinction ratio is on the order of 0.10 dB/μm, higher than reported, for instance, in (Mohsin et al, 2014), and on par with the values of (Liu, Yin and Ulin-Avila, 2011), although lower than the values obtained in (Gosciniak and Tan, 2013) or (Ren and Chen, 2019), the latter using a plasmonic slow light configuration in order to perform the modulation. It is important to highlight that the aforementioned works present highly optimized structures for operation as polarizer or modulator. The present work can serve as a starting point for optimization of dual polarizer-modulator devices based on graphene. The optimized waveguide structure mode operation layer heights were on the order of hundreds of nm, therefore within modern CMOS fabrication techniques critical feature size around 7nm (Schoot and Schift, 2017; Moore, 2018, Narasimba et al, 2017). The impact of treating graphene layer as anisotropic material (de Oliveira and de Matos, 2015; Kwon, 2014; Chang and Chiang, 2016) should be further investigated.

References

Azzam, S. I. H. et al, "Proposal of an Ultracompact CMOS-Compatible TE-/TM-Pass Polarizer Based on SoI Platform," in IEEE Photonics Technology Letters, vol. 26, no. 16, pp. 1633-1636, 15 Aug.15, 2014. [doi:10.1109/LPT.2014.2329416]

Chang, Z. and Chiang, K. S. "Experimental verification of optical models of graphene with multimode slab waveguides," Opt. Lett. 41, 2129-2132 (2016) [doi: 10.1364/OL.41.002129]

de Oliveira, R., de Matos, C "Graphene Based Waveguide Polarizers: In-Depth Physical Analysis and Relevant Parameters". Sci Rep 5, 16949 (2015) [doi:10.1038/srep16949]

Gosciniak, J., Tan, D. Theoretical investigation of graphene-based photonic modulators. Sci Rep 3, 1897 (2013) [doi:10.1038/srep01897]

Hanson, G. W. "Dyadic Green's functions and guided surface waves for a surface conductivity model of graphene" Journal of Applied Physics 103, 064302 (2008); [doi: 10.1063/1.2891452]

Hao, R., Du, W., Li, E. and Chen, H."Graphene Assisted TE/TM-Independent Polarizer Based on Mach–Zehnder Interferometer," in IEEE Photonics Technology Letters, vol. 27, no. 10, pp. 1112-1115, 15 May15, 2015. [doi: 10.1109/LPT.2015.2408375]

He, X. and Liu, J. "Flexible and broadband graphene polarizer based on surface silicon-core microfiber," Opt. Mater. Express 7, 1398-1405 (2017) [doi: 10.1364/OME.7.001398]

Hu, X. and Wang, J. "High Figure of Merit Graphene Modulator Based on Long-Range Hybrid Plasmonic Slot Waveguide," in IEEE Journal of Quantum Electronics, vol. 53, no. 3, pp. 1-8, June 2017, Art no. 7200308. [doi: 10.1109/JQE.2017.2686371]

Kawano, K. and Kitoh, T. "Introduction to Optical Waveguide Analysis", Wiley, 2001

Kim, M., Kim, S. & Kim, S. Resonator-free optical bistability based on epsilon-near-zero mode. Sci Rep 9, 6552 (2019) [doi:10.1038/s41598-019-43067-z]

Kwon, M. "Discussion of the Epsilon-Near-Zero Effect of Graphene in a Horizontal Slot Waveguide," in IEEE Photonics Journal, vol. 6, no. 3, pp. 1-9, June 2014, Art no. 6100309. [doi: 10.1109/JPHOT.2014.2326667]

Kuzmenko et al. "Universal Optical Conductance of Graphite" Phys. Rev. Lett. 100, 117401 (2008) [doi:10.1103/PhysRevLett.100.117401]

Lewkowicz, M. & Rosenstein, B. (2009). Dynamics of Particle-Hole Pair Creation in Graphene. Physical review letters. 102. 106802. [doi:10.1103/PhysRevLett.102.106802]

Liu, M., Yin, X., Ulin-Avila, E. et al. A graphene-based broadband optical modulator. Nature 474, 64–67 (2011) [doi:10.1038/nature10067]

Lu, Z. and Zhao, W. "Nanoscale electro-optic modulators based on graphene-slot waveguides," J. Opt. Soc. Am. B 29, 1490-1496 (2012) [doi: 10.1364/JOSAB.29.001490]

Mahmoud, A., Engheta, N. Wave–matter interactions in epsilon-and-mu-near-zero structures. Nat Commun 5, 5638 (2014) [doi:10.1038/ncomms6638]

Marcatili, E. A. J. "Slab-coupled waveguides," in The Bell System Technical Journal, vol. 53, no. 4, pp. 645-674, April 1974, doi: 10.1002/j.1538-7305.1974.tb02762.x

Mohsin, M. et al., "Graphene based low insertion loss electro-absorption modulator on SOI waveguide," Opt. Express 22, 15292-15297 (2014) [doi: 10.1364/OE.22.015292]

Moore, Samuel K. “EUV lithography finally ready for fabs.” IEEE Spectrum 55 (2018): 46-48. [doi: 10.1109/MSPEC.2018.8241736]

Narasimha, S. et al., "A 7nm CMOS technology platform for mobile and high performance compute application," 2017 IEEE International Electron Devices Meeting (IEDM), San Francisco, CA, 2017, pp. 29.5.1-29.5.4. [doi: 10.1109/IEDM.2017.8268476]

Nguyen, K.T. and Zhao, Y. “Integrated graphene/nanoparticle hybrids for biological and electronic applications” Nanoscale, 2014,6, 6245-6266 (2014) [doi:10.1039/C4NR00612G]

Novoselov, K.S. et al., “Electric Field Effect in Atomically Thin Carbon Films,” Science 306, 666 – 669 (2004) [doi: 10.1126/science.1102896]

Novoselov, K., Fal′ko, V., Colombo, L. et al. A roadmap for graphene. Nature 490, 192–200 (2012) [doi:10.1038/nature11458]

Okamotto, K. “Fundamentals of optical waveguides”, 2nd edition, Elsevier, 2006

Ramaswamy, V. "Strip-loaded film waveguide," in The Bell System Technical Journal, vol. 53, no. 4, pp. 697-704, April 1974. [doi: 10.1002/j.1538-7305.1974.tb02764.x]

Ren, T. and Chen, L., "Slow light enabled high-modulation-depth graphene modulator with plasmonic metasurfaces," Opt. Lett. 44, 5446-5449 (2019) [doi: 10.1364/OL.44.005446]

Santos, R.S., Martinez, M. A. G. and Giraldi, M. T. M. R. "A simple tunable TE-pass CMOS compatible polarizer," in Latin America Optics and Photonics Conference, OSA Technical Digest (Optical Society of America, 2018), paper Th3A.5. [doi: 10.1364/LAOP.2018.Th3A.5]

Schoot, J. & Schift, H. Next-generation lithography – an outlook on EUV projection and nanoimprint. Advanced Optical Technologies, 6(3-4), pp. 159-162. (2017). [doi:10.1515/aot-2017-0040]

Vakil, A., Engheta, N., “Transformation Optics Using Graphene,” Science 332, 1291 – 294 (2011) [doi: 10.1126/science.1202691]

Xiao, Yi et al., "Theoretical investigation of optical modulators based on graphene-coated side- polished fiber," Opt. Express 26, 13759-13772 (2018) [doi: 10.1364/OE.26.013759]

Xu et al. “Complex refractive index tenability of graphene at 1550 nm wavelength” Appl. Phys. Lett. 106, 031109 (2015) [doi:10.1063/1.4906349]

Yin, X. et al. "Ultra-compact TE-pass polarizer with graphene multilayer embedded in a silicon slot waveguide," Opt. Lett. 40, 1733-1736 (2015) [doi: 10.1364/OL.40.001733]

Yin, X. et al, "Ultra-Broadband TE-Pass Polarizer Using a Cascade of Multiple Few-Layer Graphene Embedded Silicon Waveguides," J. Lightwave Technol. 34, 3181-3187 (2016). [doi: 10.1109/JLT.2016.2547896]

Zhang, Y., Brar, V., Girit, C. et al. Origin of spatial charge inhomogeneity in graphene. Nature Phys 5, 722–726 (2009). [doi: 10.1038/nphys1365]

Zhang, T. et al. "Ultra-compact polarization beam splitter utilizing a graphene-based asymmetrical directional coupler," Opt. Lett. 41, 356-359 (2016) [doi: 10.1364/OL.41.000356]

Ziolkowski, R. W. “Propagation in and scattering from a matched metamaterial having a zero index of refraction” Phys. Rev. E 70, 046608 (2004) [doi: 10.1103/PhysRevE.70.046608]

Declarations

Funding: Not Applicable.

Conflicts of interest/Competing interests: Not applicable.

Availability of data and material: Not applicable.

Code availability: Not applicable.

Figures

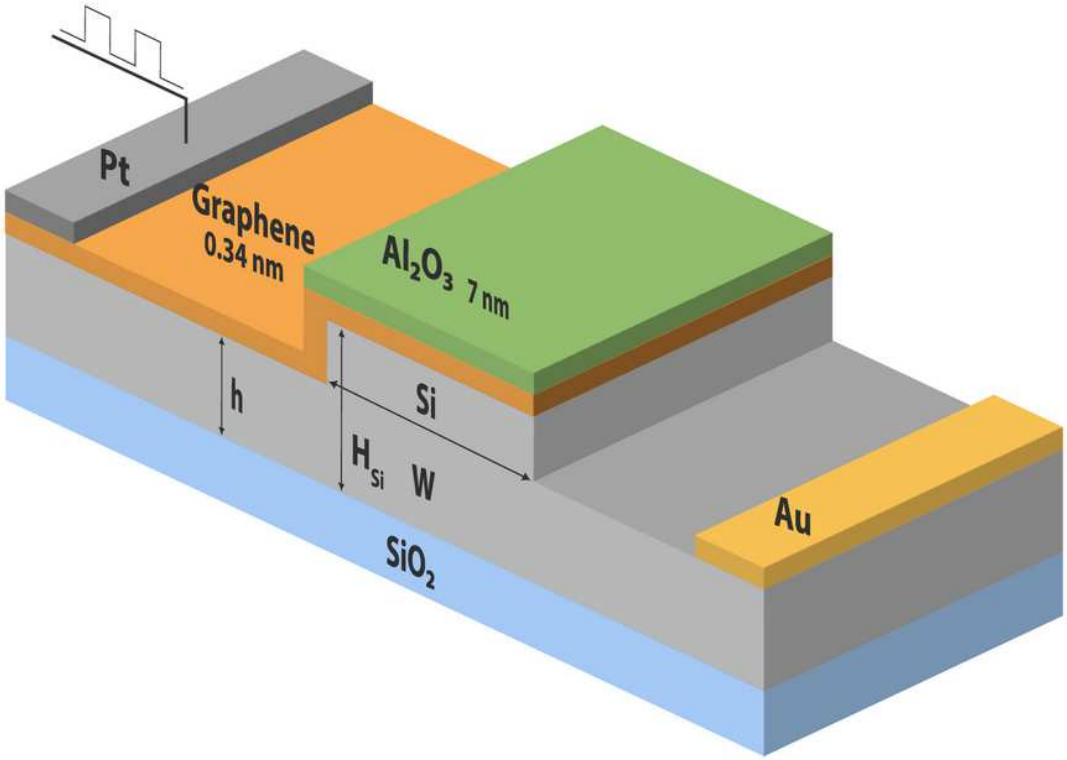

Figure 1

Rib waveguide used for analysis. W = 900 nm and h = 150 nm

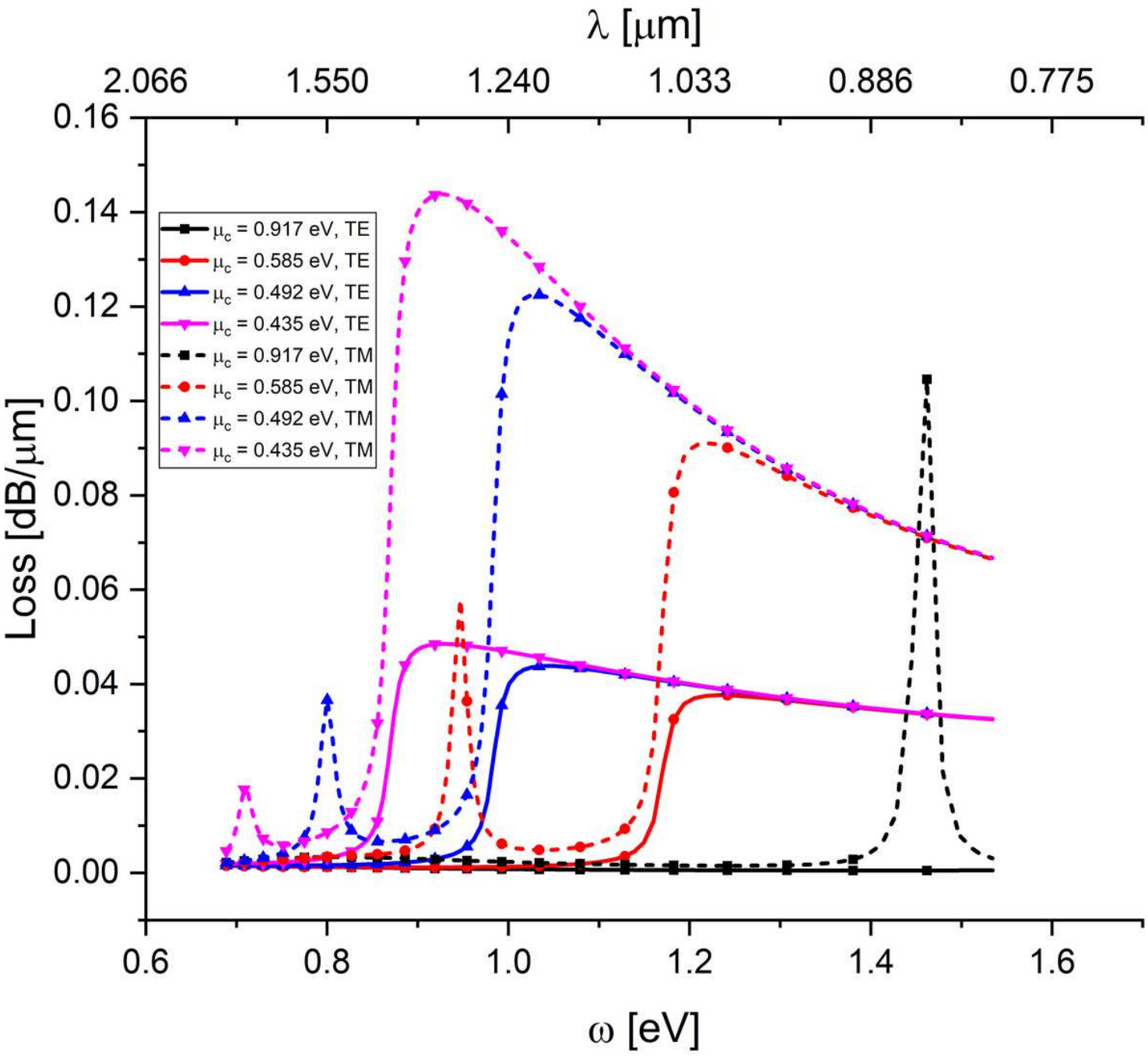

Figure 2

Losses (in dB/μm) as a function of wavelength , and correspondent value in eV, for the fundamental TE mode (solid lines) and TM mode (doted lines), for the chemical potentials of 0.435 eV (inverted triangle), 0.492 eV (triangle), 0.585 eV (circle) and 0.917 eV.(square)

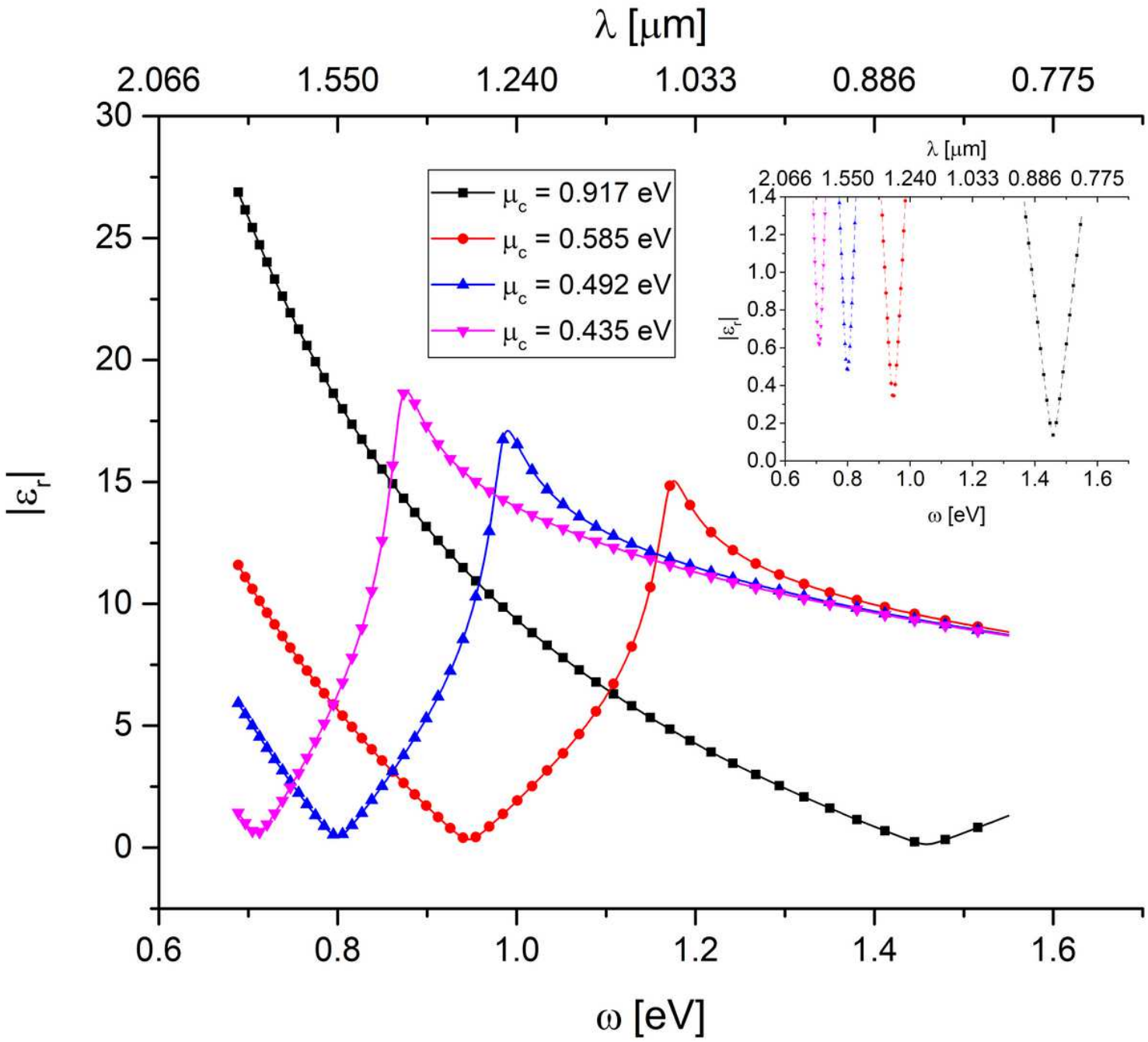

Figure 3

Absolute value of graphene permittivity as a function of wavelength, for the chemical potentials of 0.435 eV, 0.492 eV, 0.585 eV and 0.917 eV. Inset: magnification of epsilon near-zero region.

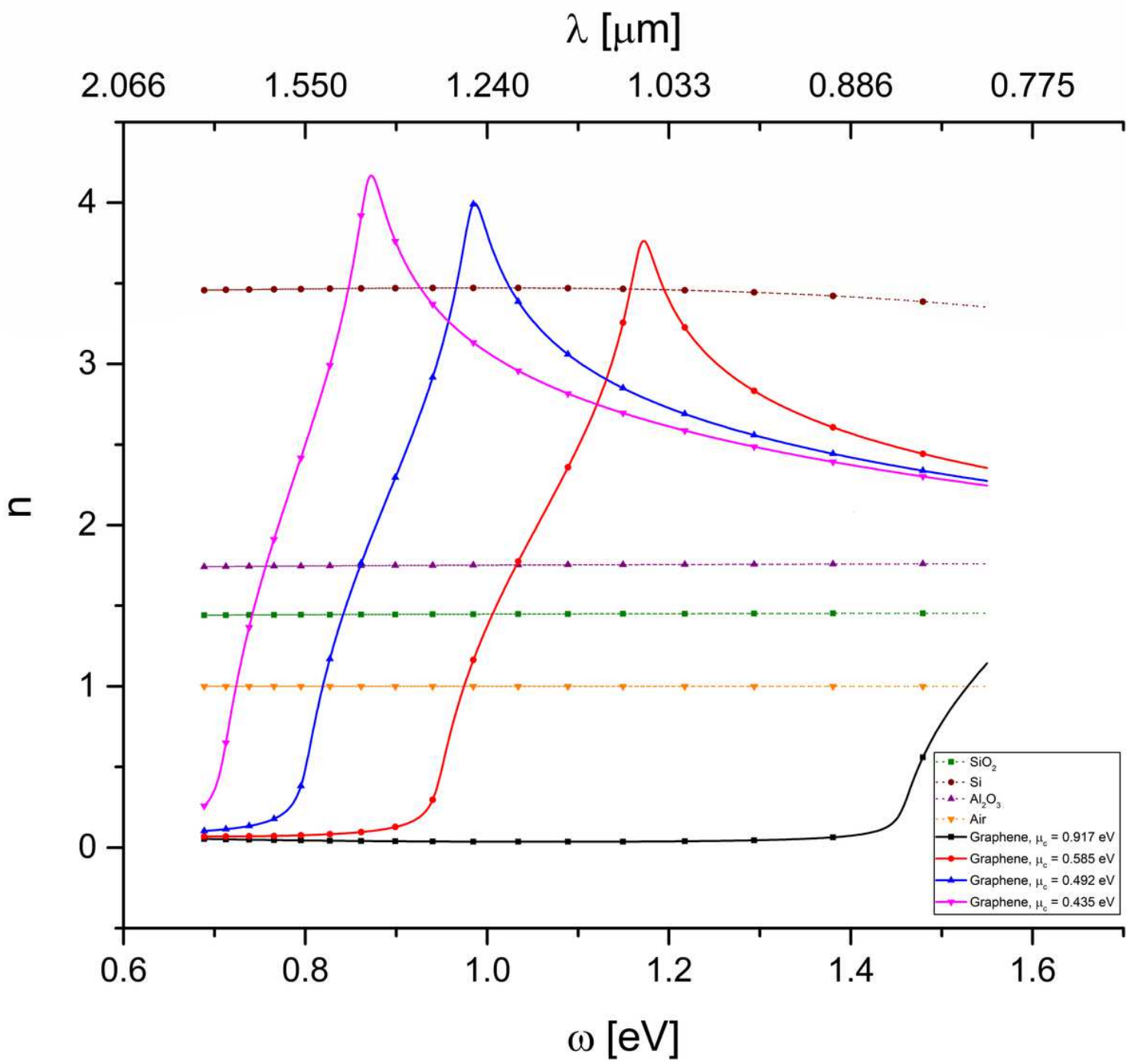

Figure 4

Real part of graphene refractive index (solid lines) as a function of wavelength, for the chemical potentials of 0.435 eV (inverted triangle) , 0.492 eV (triangle), 0.585 eV (circle) and 0.917 eV (square) , and the refractive SiO2 (dotted line-square), Si (dotted line-circle) and Al2O3 (dotted line-triangle) layers.

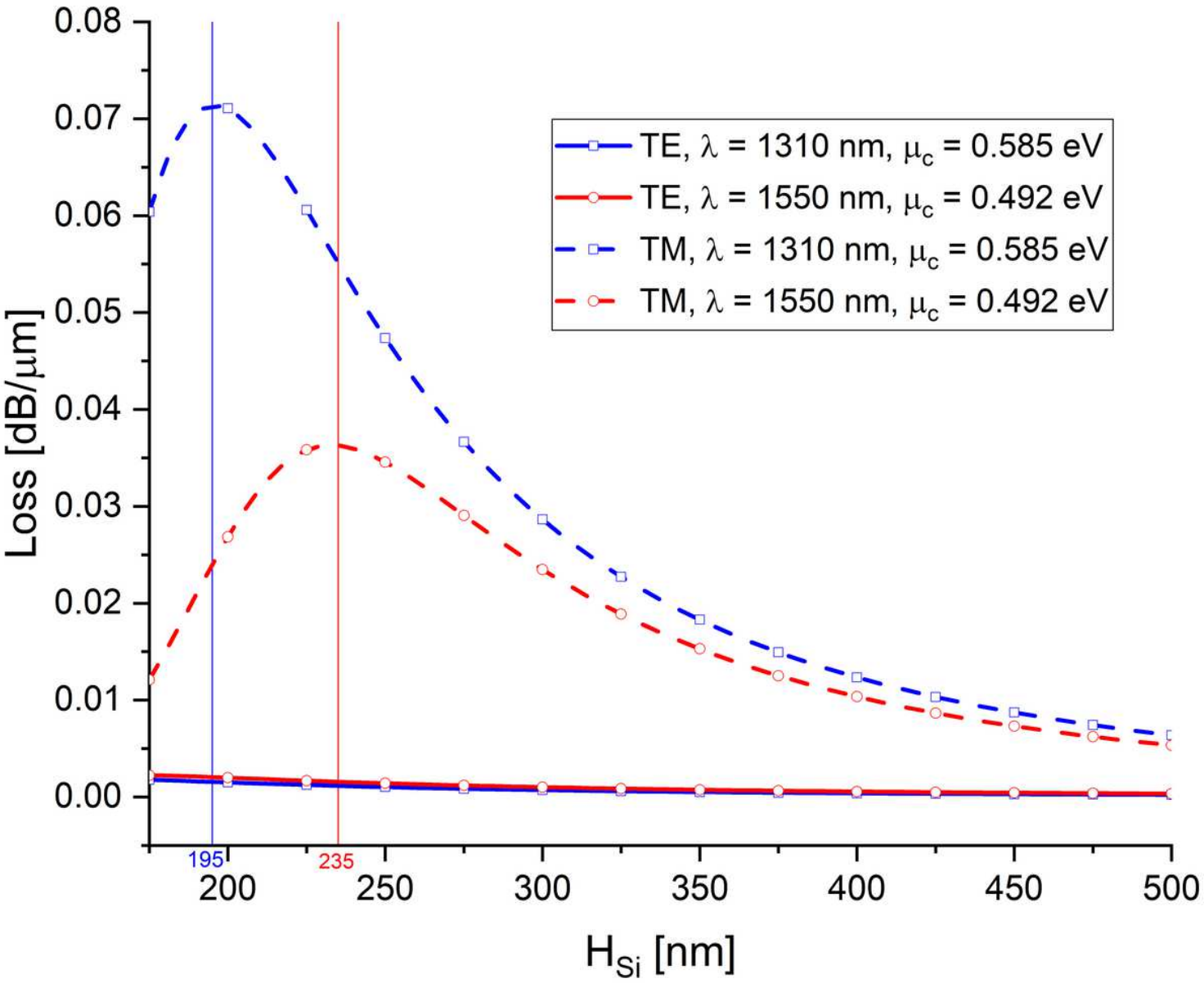

Figure 5

TE (solid line) and TM (dotted lines) modes normalized absorption coefficient as a function of silicone core height for λ = 1310 nm and λ = 1510 nm.

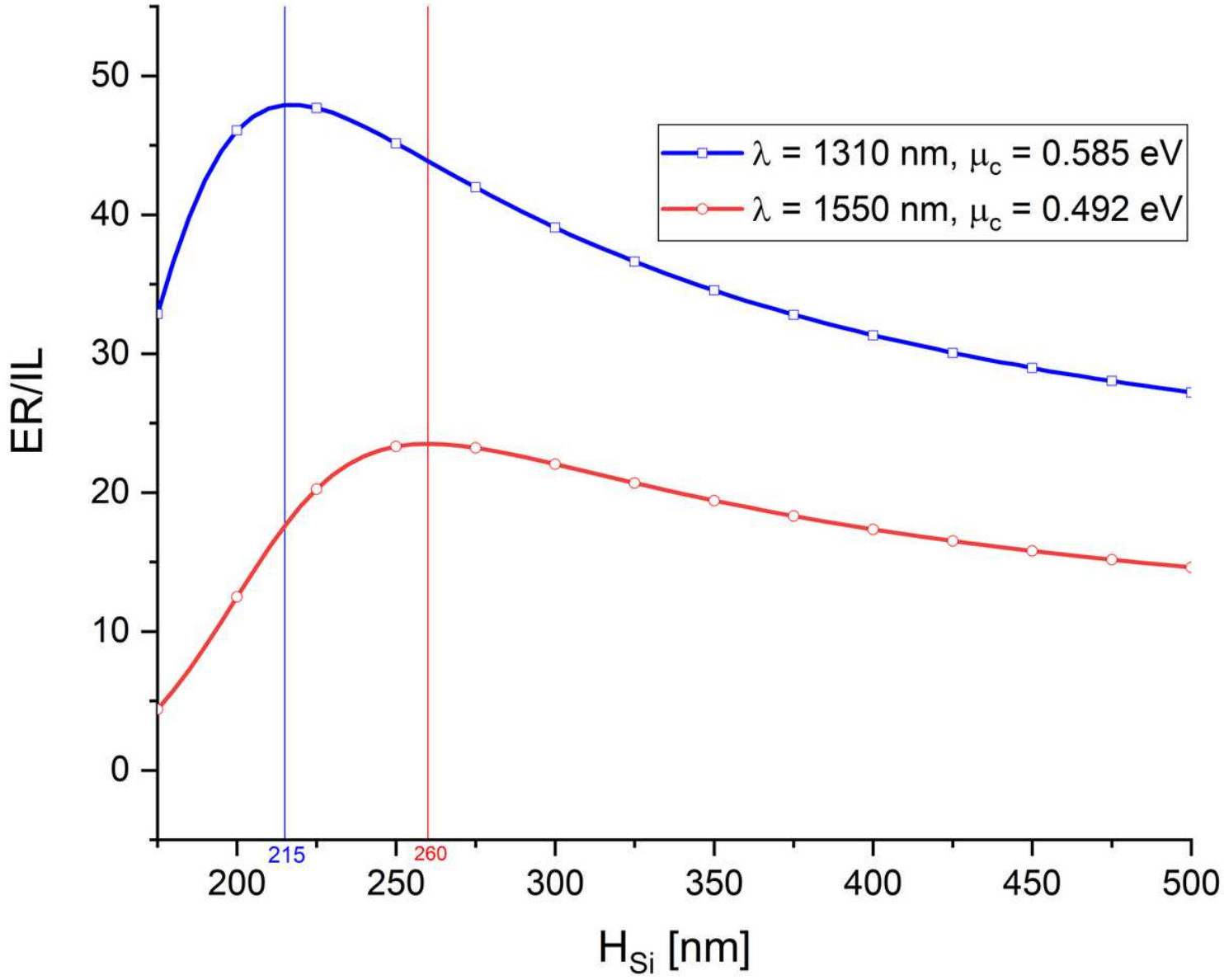

Figure 6

Figure of merit as a function of silicon core height for λ = 1310 nm and λ = 1510 nm.

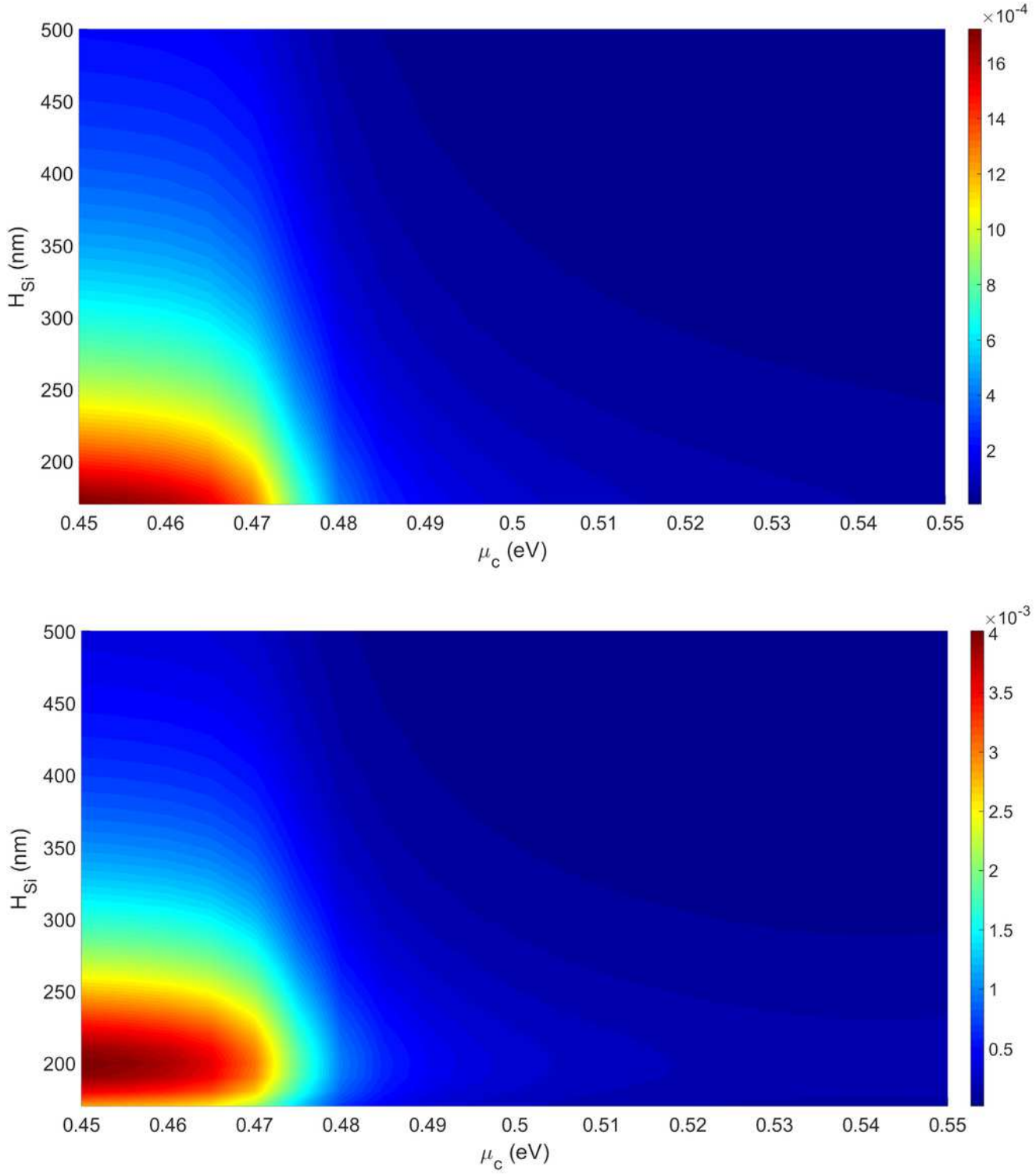

Figure 7

Normalized absorption coefficient as a function of silicon core height and chemical potential for λ = 1310 nm nm. (a) TE mode (b) TM mode

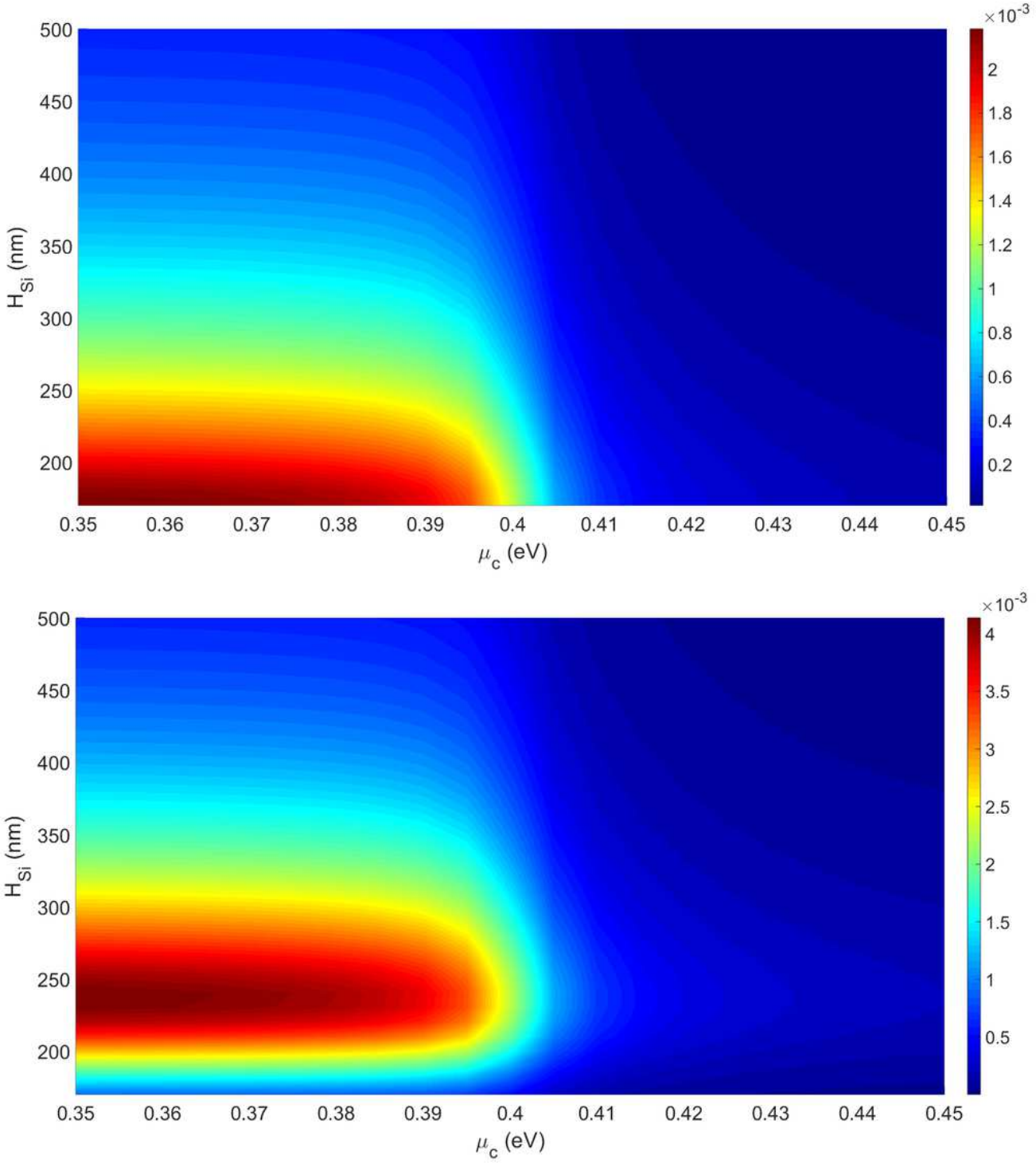

Figure 8

Normalized absorption coefficient as a function of silicon core height and chemical potential for λ = 1550 nm. (a) TE mode (b) TM mode

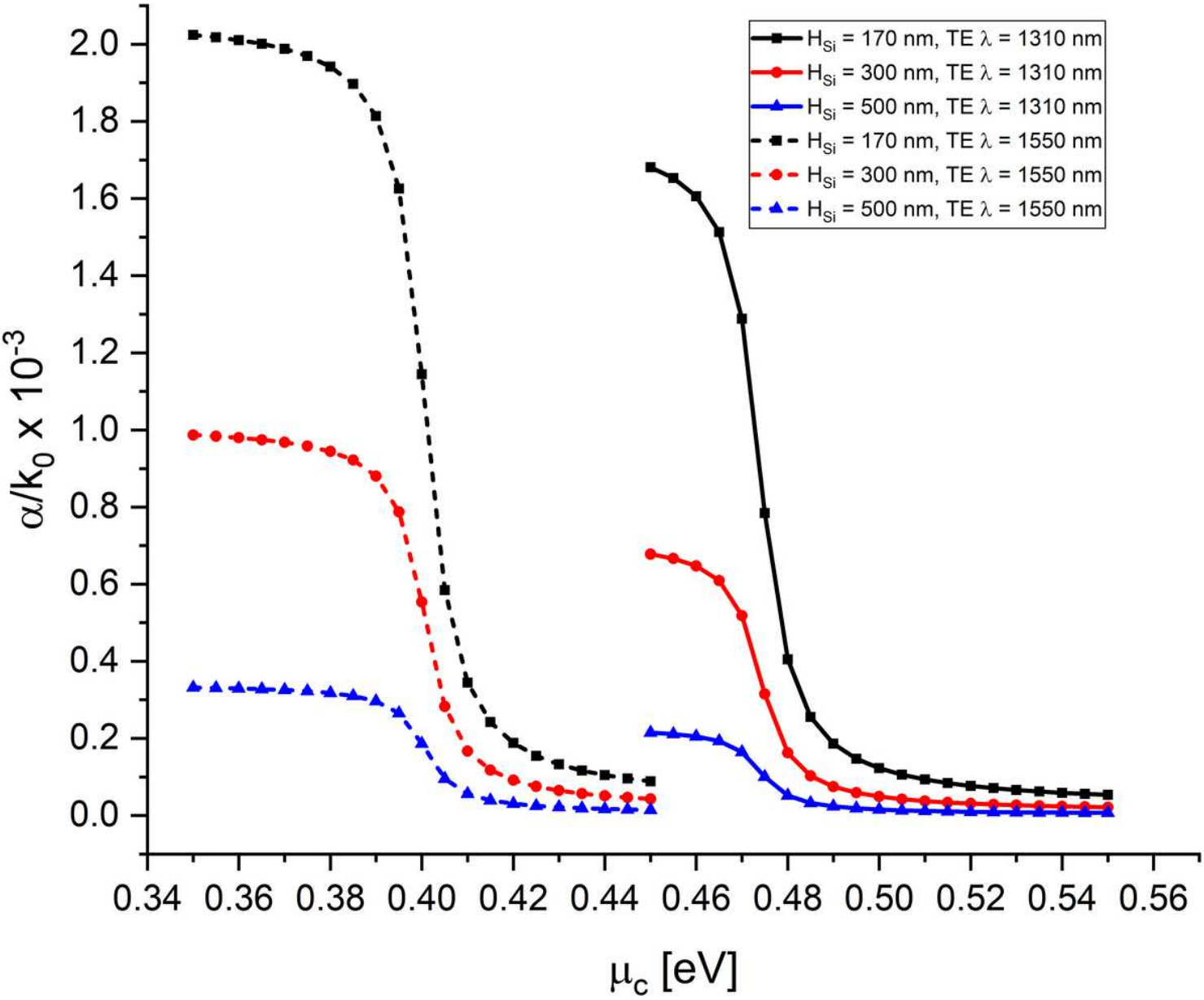

Figure 9

Normalized absorption coefficient as a function of chemical potential, for TE modes, for three different values of silicon core height, at λ = 1310 nm and λ = 1550 nm wavelength

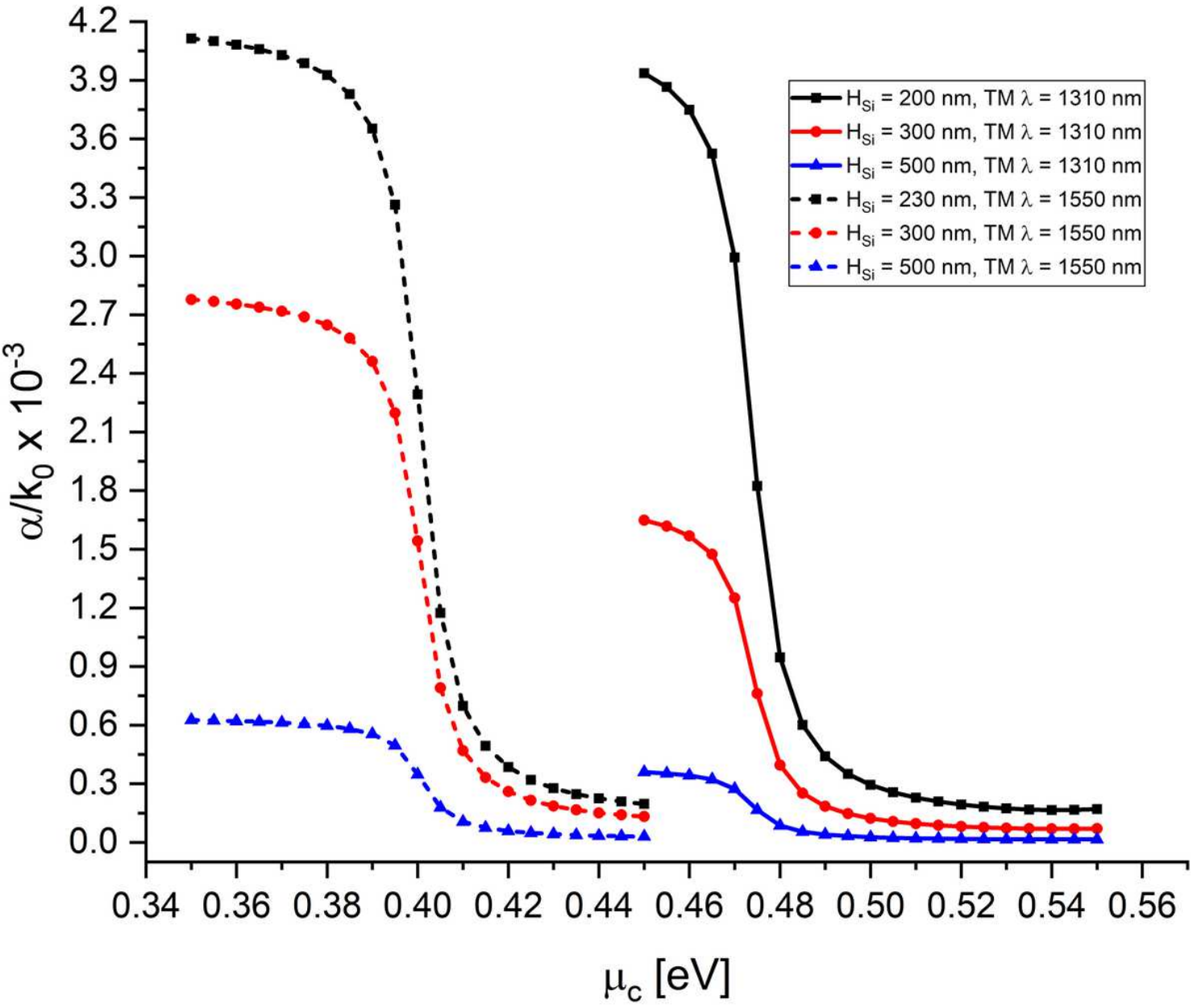

Figure 10

Normalized absorption coefficient as a function of chemical potential, for TM modes, for three different values of silicon core height, at λ = 1310 nm and λ = 1550 nm wavelength

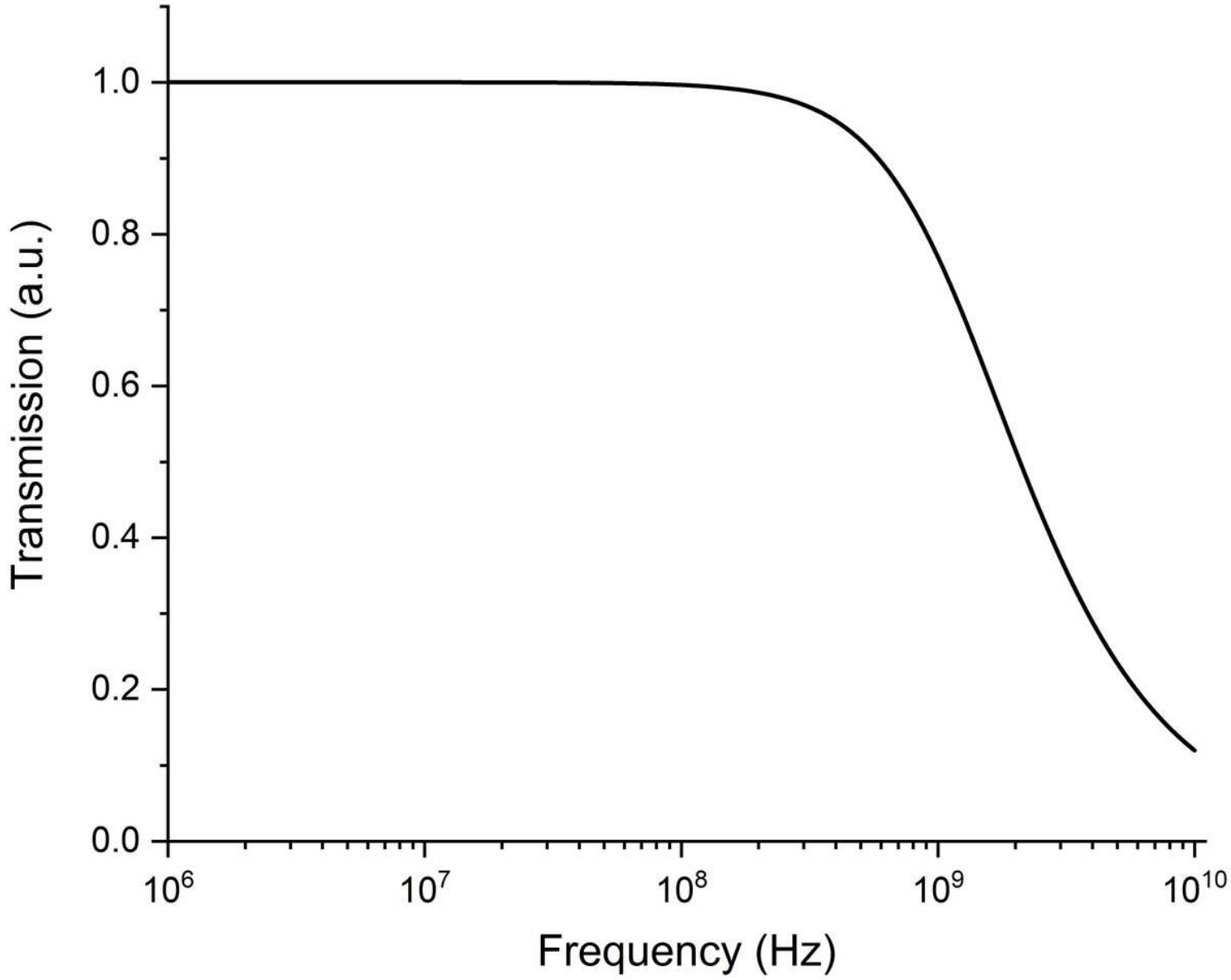

Figure 11

Estimated frequency response of the structure

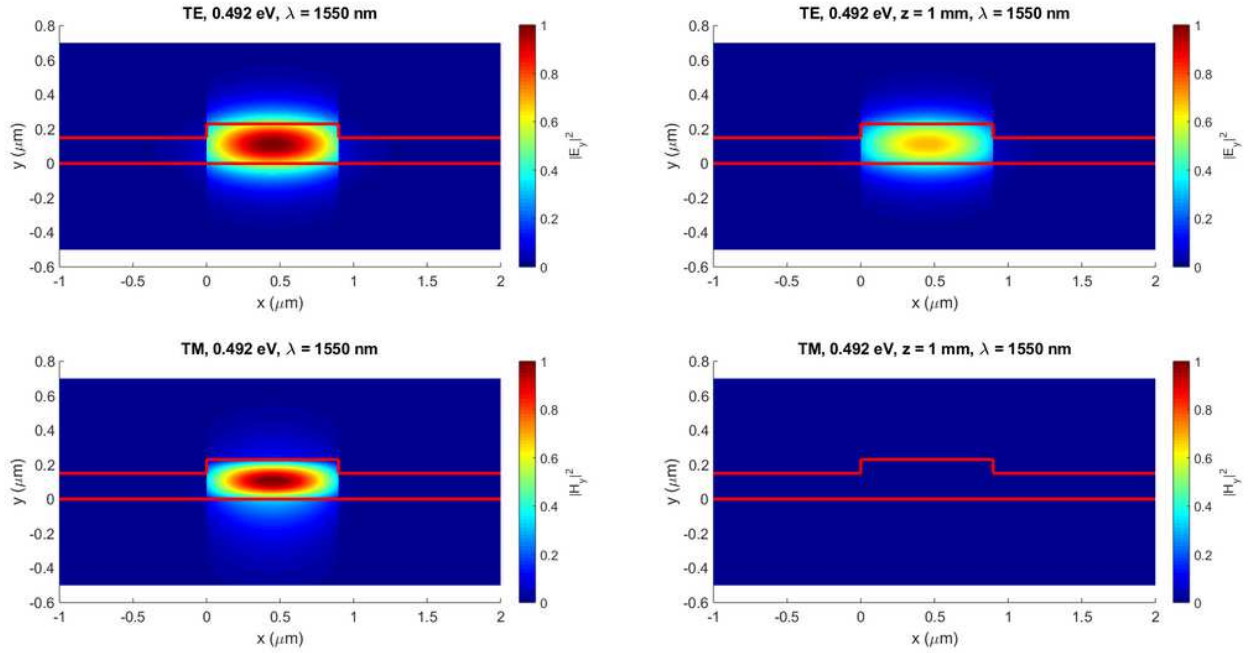

Figure 12

Field intensity for TE (upper row) and TM (lower row) modes for polarizer operation, at the beginning of the waveguide (first column) and after 1 mm (second column) for 1550 nm and 0.492 eV chemical potential

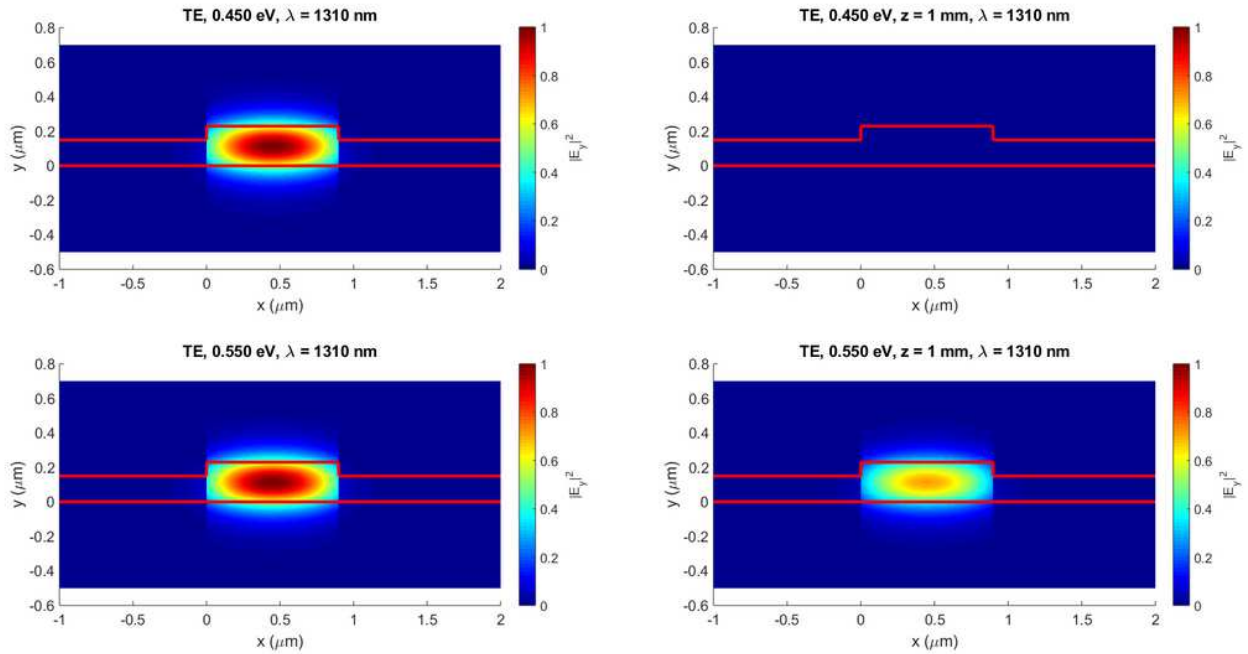

Figure 13

Field intensity for TE mode for modulator operation, at the beginning of the waveguide (first column) and after 1 mm (second column) at 0.450 eV (upper row) and 0.550 eV (lower row) for 1310 nm